# Nonlinear evolution of nonuniformly heated falling liquid films

Benoit Scheid
*Microgravity Research Center, Université Libre de Bruxelles C.P. 165/62, 1050 Brussels, Belgium and Department of Mechanical Engineering, Technion-Israel Institute of Technology, Haifa 32000, Israel*

Alexander Oron[a)]
*Department of Mechanical Engineering, Technion-Israel Institute of Technology, Haifa 32000, Israel*

Pierre Colinet[b)]
*Microgravity Research Center, Université Libre de Bruxelles C.P. 165/62, 1050 Brussels, Belgium*

Uwe Thiele
*Instituto Pluridisciplinar, Universidad Complutense, Paseo Juan XXIII, 1, 28040 Madrid, Spain and Department of Physics, University of California, Berkeley, California 94720-7300*

Jean Claude Legros
*Microgravity Research Center, Université Libre de Bruxelles C.P. 165/62, 1050 Brussels, Belgium*

(Received 3 December 2001; accepted 27 August 2002; published 18 October 2002)

The present theoretical study focuses on the dynamics of a thin liquid film falling down a vertical plate with a *nonuniform, sinusoidal* temperature distribution. The results are compared to those obtained in the case of the *uniform* temperature distribution. The governing evolution equation for the film thickness profile based on long-wave theory accounts for two instability mechanisms related to thermocapillarity. The first mechanism is due to an inhomogeneity of the temperature at the liquid–gas interface induced by perturbations of the film thickness, when heat transfer to the gas phase is present, while the second one is due to the nonuniform heating imposed at the plate and leads to steady-state deformations of the liquid–gas interface. For a moderate nonuniform heating the traveling waves obtained in the case of a uniform heating are modulated by an envelope. When the temperature modulation along the plate increases the shape of the liquid–gas interface becomes ''frozen'' and the oscillatory traveling wave regime is suppressed. The enhancement of the heat transfer due to permanent deformations and traveling waves is also assessed. The latter is found to have no significant effect on the heat transfer coefficient, while the former can increase it significantly. A good agreement between the theoretical model and the experimental data obtained for a step-wise temperature distribution at the plate is found and the reason for discrepancies is explained. © *2002 American Institute of Physics.* [DOI: 10.1063/1.1515270]

## I. INTRODUCTION

The flow of a liquid film on a tilted solid plate has many significant engineering applications in material processing, biomedical engineering, food and chemical industries. Such flows are often encountered in evaporators for separation of multicomponent mixtures where fluids are temperature-sensitive, and hence a low thermal driving force is required. In thin-film flows, the most widely observed phenomena, such as formation of surface waves, breaking of a stream into rivulets, and evaporation with termination of the liquid layer at a contact line, are caused by various interfacial instability mechanisms. Therefore, the understanding of the nonlinear dynamics of these phenomena will help to improve predictions of heat and mass transfer rates.

A horizontal thin layer of liquid on a solid plate can be subject to a long-wave thermocapillary instability when it is heated from below. This instability mode first studied by Scriven and Sternling[1] is associated with the modification of the basic temperature at the free surface by the surface deformation. The deformation is opposed mainly by gravity and for disturbances of a sufficiently short wavelength also by surface tension. Therefore, this instability mode occurs when the thermocapillary force overcomes the force due to hydrostatic pressure[1] for

$$\frac{G}{3} < \frac{BM}{2Pr(1+B)^2}.$$

Here $G$ is the Galileo number, $B$ is the Biot number, $Pr$ is the Prandtl number and $M$ is the Marangoni number (see Sec. II for definitions). Because $G \sim h^3$, while $B \sim h$ and $M \sim h$ the layer will be unstable for a sufficiently small film thickness $h$. The reader is referred to the comprehensive book of Colinet *et al.*[2] for more detail on this topic. For this mode of thermocapillary instability the disturbance has no preferred direction as long as the layer is kept horizontal. On the contrary, when a flow takes place, this isotropy is broken

[a)]Author to whom correspondence should be addressed. Telephone: (972) 4 829 3474; fax: (972) 4 832 4533. Electronic mail: meroron@tx.technion.ac.il
[b)]Chargé de recherches, Fonds National de la Recherche Scientifique (Belgium).

 

and the instability manifests itself in waves. Furthermore, when the layer is tilted, it can become unstable even without heat transfer. This isothermal mode of instability, often called surface-wave instability, was identified by Yih[3] and Benjamin.[4] Except for very small angles of inclination, the gravity-driven surface waves with a wavelength much larger than the film thickness cause instability first.[5] The disturbance originates at the free surface where vorticity is produced by the basic flow shear stress.[6,7] Owing to the effects of inertia, the perturbation vorticity tends to be advected downstream relative to the deflection of the free surface so as to cause instability. This shift is opposed by hydrostatic and surface tension forces. Since the latter one is negligible for large-wavelength disturbances, in this limit the instability manifests itself when the effect of inertia overcomes the hydrostatic force expressed by the relation[3]

$$R > \tfrac{5}{2}\cot\beta.$$

Here $R$ is the Reynolds number and $\beta$ is the angle of inclination from the horizontal. In the limiting case of a vertical plate ($\beta=\pi/2$) the stabilizing hydrostatic pressure vanishes and the interface is always unstable, i.e., for all film thicknesses. Experiments performed by Liu *et al.*[8,9] for this situation are in good agreement with the critical Reynolds number, growth rates and wave velocities resulting from linear stability analysis.

Since the instabilities in thin films appear in the form of long interfacial waves, nonlinear analyzes using long-wave evolution equation of the Benney[10] type turns out to be useful. Oron and Gottlieb[11] showed by comparison with direct numerical simulations of the full hydrodynamic equations that the Benney equation (BE) is valid in the parameter domain adjacent to the linear stability threshold of the system. Burelbach *et al.*[12] studied long-wave instabilities in a horizontal layer in the presence of evaporation, vapor recoil, and van der Waals forces. Joo *et al.*[13] generalized this study to include the effect of mean flow by tilting the plate in the absence of van der Waals forces and analyzed the nonlinear dynamics by numerically solving the pertinent evolution equation. To obtain an extended overview of the dynamics of thin liquid films the reader is referred to the review paper of Oron *et al.*[14]

However, when the convective effects become significant, the BE (at any order of the asymptotic expansion) fails to serve as a good model for spatiotemporal evolution of falling films. The solutions of the BE then significantly deviate from those of the full hydrodynamic equations and finally at some distance beyond the stability threshold of the system, its solutions undergo a blow-up in a finite-time[11,15,16] despite the regularizing effect of surface tension. Since Shkadov,[17] the integral boundary-layer (IBL) model using the Pohlhausen–von-Kármán averaging method appears to be suitable in describing the dynamics of falling films for large Reynolds numbers, as such a model typically involves more than one evolution equation, accounting for the kinematic variable, the film thickness, as well as for a dynamic one, the local flow rate. Even though the IBL equations do not experience any blowup, they do not properly predict the linear stability threshold, as the BE does. The compromise between these models was recently found by Ruyer-Quil and Manneville[18,19] by combining a gradient expansion to weighted-residual techniques with polynomials as test functions. In this new context, we will address in the present study the range of validity of the BE as a mathematical model for description of the dynamics of falling vertical films in terms of the relevant parameters.

Tan *et al.*[20] examined the steady thermocapillary flow in thin liquid layers on a nonuniformly heated horizontal solid plate. They showed that a continuous steady profile of the liquid layer can be sustained only if the value of the dynamic Bond number that measures the balance between gravity and thermocapillary forces, is higher than a certain critical value. Moreover, inclusion of the van der Waals forces in the analysis, for a very thin film, either leads to spontaneous film rupture or prevents the occurrence of any dry spot on the microscopic scale, depending on the attractive or repulsive character of this force, hence on the nature of liquid and plate. Small perturbations of uniform heating and their effect on the dynamics of the film were also studied by Van Hook *et al.*[21] for a horizontal layer ($\beta=0$). They showed that nonuniformity in heating produces a steady-state deformation for any temperature difference across the layer. This steady-state deformation becomes unstable to the long-wavelength instability earlier than in the absence of nonuniformity. Moreover, the nonuniformity of the plate temperature determines the location of the dry spot and the elevated region to form at the minimum and maximum of the steady-state deformation, respectively. Recently, Or *et al.*[22] found a way to suppress the long-wavelength disturbances by applying a feedback control to the temperature at the substrate.

In the area of heat transfer enhancement a nonuniform heating of falling liquid films is thought to be a promising solution since it induces steady-state deformations of the liquid–gas interface which are beneficial to the heat transfer process.[23] It is then essential to understand the influence of nonuniformities in heating, and whether they can either improve the heat transfer through the film or hinder it by propelling the film to its rupture. To our knowledge, few studies exist in literature in this field of research. Miladinova *et al.*[24,25] considered the effect of a constant temperature gradient imposed at the plate for an adiabatic liquid–gas interface ($B=0$) and high Marangoni number. They studied the influence of thermocapillarity on the amplitudes and phase speeds of surface waves resulting from instability and found from linear analysis that a weak increase in heating downstream produces a decrease in the stability threshold, while a decrease of the temperature plays a stabilizing role. In the nonlinear regime, they found finite-amplitude waves, the shape of which depends mostly on the mean flow velocity, while the amplitude is influenced by the thermocapillarity.

Recent experimental studies focused on thin films falling down a locally heated plate revealed the occurrence of steady-state deformations.[26,27] In this case, the localized temperature gradient imposed at the plate and aligned with the flow induces a steady horizontal bump shape of the liquid–gas interface due to the thermocapillary effect. In an attempt to explain the phenomenon Kabov *et al.*[28,29] proposed a model taking into account variations of surface tension and

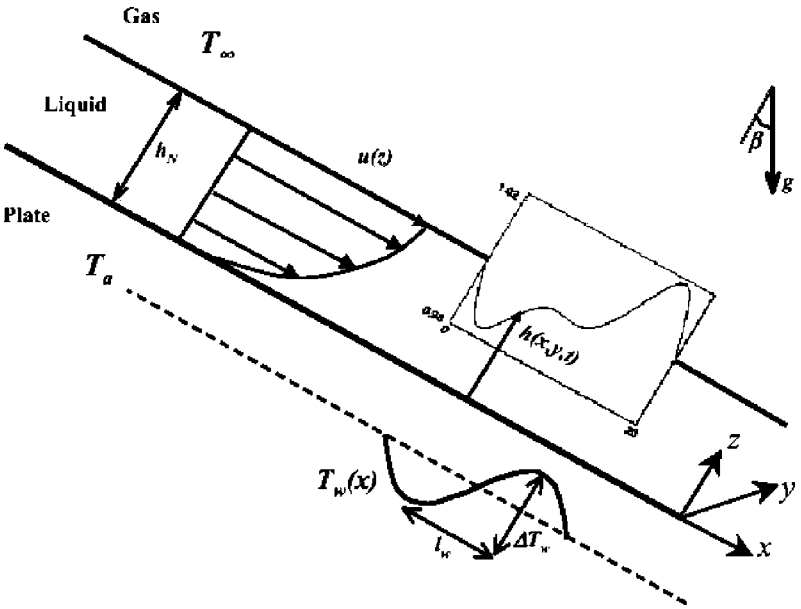


FIG. 1. Geometry of the problem $\bar{u}(\bar{z})$ indicates the Nusselt velocity profile of the liquid film, $h_N$ is the mean film thickness, $g$ is the gravity acceleration, $\beta$ is the inclination angle of the plate with respect to the horizontal, $\bar{T}_\infty$ is the temperature of the passive gas and $\bar{T}_a$ is the average temperature of the plate. The function $\bar{T}_w(\bar{x})$ represents the nonuniform plate temperature distribution around $\bar{T}_a$ and $\Delta\bar{T}_w$ is the characteristic temperature difference applied at the plate along the length $l_w$. The liquid–gas interface is deformable as zoomed in the inset frame, where $\bar{z}=\bar{h}(\bar{x},\bar{y},\bar{t})$ is the interface location. The bars over variables are omitted in the graph.

viscosity with temperature. They obtained an excellent quantitative agreement with the experimental data, especially in the downstream of the bump, where they explained a film thinning below the average thickness by an increase of the fluid mobility induced by the temperature decrease of the liquid viscosity.

The present study focuses on the evolution of a thin liquid film falling down a vertical plate in which a periodic array of heaters is embedded. Using a Benney-type expansion we derive in Sec. II an evolution equation for the film thickness accounting for the effect of nonuniform heating. In Sec. III, stationary solutions of this evolution equation are calculated either in a moving reference frame in the case of uniform heating or in a fixed reference frame in the case of nonuniform heating. The first case allows for traveling wave solutions, while the second one yields steady-state deformations. Two kinds of boundary conditions are considered, corresponding to either a given temperature distribution, or a given heat flux at the plate. We show that only the former is appropriate to take into account the coupling between the thermocapillary instability and steady-state deformations. As we will see, this coupling causes a variety of nonlinear phenomena, such as oscillatory regimes or chaotic patterns. To describe these dynamic phenomena we solve numerically in Sec. IV the two-dimensional evolution equation using the Newton–Kantorovich method. The periodic temperature distribution at the plate is chosen to be sinusoidal and the resulting dynamics is compared to the case of a uniform heating with the same average temperature. An important result is that for a sufficiently strong temperature nonuniformity at the plate, the shape of the liquid–gas interface becomes ''frozen,'' suppressing the oscillatory traveling wave regime. In Sec. V we estimate the enhancement of the heat transfer due to those permanent deformations, as well as due to additional oscillations. The influence of the magnitude of the average temperature is also considered. Section VI presents a description of the experimental results and their comparison with the results obtained from our model. Measurements of the bump shape are compared with the calculated stationary solutions and with the results of numerical time integrations of the full evolution equation. We note that the linear stability analysis of such two-dimensional stationary deformations with respect to transverse disturbances was recently performed by Skotheim, Thiele, and Scheid[30] in the limit of low Reynolds number flows. They found a three-dimensional instability leading to the formation of a rivulet pattern aligned with the flow as observed first experimentally by Kabov.[23,31] However, this is beyond the scope of the present work. Section VII is devoted to summary and concluding remarks.

## II. STATEMENT OF THE PROBLEM AND EVOLUTION EQUATION

We investigate here the two-dimensional dynamics of a thin liquid film falling down a plate tilted by an angle $\beta$ from the horizontal, under the gravity acceleration $g$. This plate is maintained at the nonuniform temperature $\bar{T}=\bar{T}_a+\bar{T}_w(\bar{x})$, where $\bar{T}_a$ is the average plate temperature and $\bar{T}_w(\bar{x})$ is a periodic temperature distribution with a zero average. In what follows the variables with and without bars denote dimensional and dimensionless quantities, respectively.

The coordinates $\bar{x}$ and $\bar{z}$ designate the directions parallel and normal to the flow, respectively. The geometry of the problem is presented in Fig. 1. The ambient gas phase is assumed to be passive and held at the uniform temperature $\bar{T}_\infty$ and pressure $\bar{p}_\infty$. The fluid properties are the density $\rho$, kinematic viscosity $\nu$, thermal diffusivity $\chi$, thermal conductivity $k$, the heat transfer coefficient from the liquid to the gas $\alpha_h$, the surface tension $\sigma_\infty$ at the gas temperature and the absolute value of its temperature-derivative $\gamma$, assuming that the surface tension linearly decreases with the temperature, $\sigma=\sigma_\infty-\gamma(\bar{T}_i-\bar{T}_\infty)$, where $\bar{T}_i$ is the interfacial temperature. As in most studies of the Marangoni instability the fluid viscosity is assumed to be temperature-independent.

The characteristic temperature differences applied along the plate and across the liquid layer are $\Delta\overline{T}_w=\overline{T}_{w_{\max}}-\overline{T}_{w_{\min}}$ and $\Delta\overline{T}=\overline{T}_a-\overline{T}_\infty$, respectively. The dimensionless forms of the temperature in the film and at the plate are, respectively,

$$T=\frac{\overline{T}_f-\overline{T}_\infty}{\Delta\overline{T}_w},\quad T_w=\frac{\overline{T}_w}{\Delta\overline{T}_w},$$

where $\overline{T}_f$ is the temperature of the film. The ratio between the two characteristic temperature differences of the problem is defined by

$$\delta=\frac{\Delta\overline{T}}{\Delta\overline{T}_w}.$$

The characteristic lengths in the $\overline{x}$ and $\overline{z}$ directions are the characteristic wave length $l$ of interfacial disturbances and the mean film thickness $h_N$, respectively. The interfacial distortions are considered to be of ''long scale'' if the parameter

$$\varepsilon=\frac{h_N}{l}\ll 1.$$

The dimensionless spatial coordinates are introduced by

$$x=\varepsilon\frac{\overline{x}}{h_N}\quad\text{and}\quad z=\frac{\overline{z}}{h_N}.$$

We introduce also the length $l_w$ over which the temperature difference $\Delta\overline{T}_w$ is applied at the plate. Its dimensionless form will be $L_w=l_w/l$. Finally, the liquid–gas interface is assumed to be material and described by the function $\overline{h}=\overline{h}(\overline{x},\overline{t})$, where $\overline{t}$ is time. The dimensionless forms of these variables are

$$h=\frac{\overline{h}}{h_N}\quad\text{and}\quad t=\frac{\varepsilon\nu\overline{t}}{h_N^2}.$$

The approach used here is based on the well-known Benney equation[10,14] derived in the context of thin film theory. This equation describes the nonlinear dynamics of a liquid film of thickness $h(x,t)$ falling down an inclined plate in the isothermal conditions. In the present study the contributions of a nonuniform heating of the plate and differential heating across the film are incorporated into the Benney equation. The complete derivation of the evolution equation from the Navier–Stokes, energy and continuity equations complemented by the appropriate boundary conditions is given in the Appendix. Nevertheless, we show hereafter the integration of the energy equation along with the appropriate boundary conditions, since it has a primary importance in the following.

The energy equation written at leading order of the asymptotic expansion for $\varepsilon\to 0$ is

$$T_{zz}=0, \tag{1}$$

and the corresponding thermal boundary conditions read

$$T=\delta+T_w\quad\text{at}\quad z=0, \tag{2}$$

$$T_z+BT=0\quad\text{at}\quad z=h, \tag{3}$$

where the subscript $z$ stands for the partial derivative with respect to $z$ and $B=\alpha_h h_N/k$ is the Biot number. Therefore, Eqs. (1)–(3) yield the temperature distribution in the film

$$T=(\delta+T_w)\left(1-\frac{Bz}{1+Bh}\right), \tag{4}$$

from which one finds the temperature distribution at the liquid–gas interface $z=h$

$$T_i(x,t)=\frac{\delta+T_w(x)}{1+Bh(x,t)}. \tag{5}$$

The interfacial thermocapillary stress is thus given in dimensionless form by

$$\Sigma_x=\frac{Ma}{Pr}T_{i_x}, \tag{6}$$

where the subscript $x$ stands hereafter for the partial derivative with respect to $x$

$$Ma=\frac{\gamma\Delta\overline{T}_w h_N}{\rho\nu\chi}\quad\text{and}\quad Pr=\frac{\nu}{\chi}$$

are the Marangoni and Prandtl numbers, respectively.

Finally, the evolution equation containing an additional thermocapillary term is obtained (see the Appendix)

$$h_t+Rh^2h_x+\varepsilon\left(\frac{2}{15}R^2h^6h_x-C\frac{h^3}{3}h_x+S\frac{h^3}{3}h_{xxx}-M_w\frac{h^2}{2}T_{i_x}\right)_x+O(\varepsilon^2)=0, \tag{7}$$

where

$$R=G\sin\beta,\quad C=G\cos\beta,$$

$$S=\varepsilon^2\frac{\sigma_\infty h_N}{\rho\nu^2}\quad\text{and}\quad M_w=\frac{Ma}{Pr},$$

are the Reynolds, the hydrostatic pressure, the surface tension and the *effective* Marangoni numbers, respectively. $G=gh_N^3/\nu^2$ is the Galileo number. In the above equation, the parameters $R$, $C$, $S$, and $M_w$, as well as $h$, $T_i$ and their $x$-derivatives, are all assumed to be of order one, i.e., $O(1)$. Furthermore, the nonuniformity of the heating is assumed to induce deformations that have a length scale comparable to that of the interfacial disturbances, so that $L_w=O(1)$. Note that $S=R^{1/3}(\varepsilon^2 Ka)$ where $Ka=\sigma_\infty/(\rho g^{1/3}\nu^{4/3})$ is the Kapitza number. The present study is carried out for the case of a vertical plate only, $\beta=\pi/2$, therefore, $C=0$ and the hydrostatic pressure term in Eq. (7) vanishes.

Substituting the plate temperature $T_i$ given by Eq. (5) transforms Eq. (7) to the form

$$h_t + Rh^2 h_x + \varepsilon\left[\frac{2}{15}R^2 h^6 h_x + S\frac{h^3}{3}h_{xxx} + BM_w\frac{h^2}{2}\frac{(\delta+T_w)h_x}{(1+Bh)^2} - M_w\frac{h^2}{2}\frac{T_{w_x}}{1+Bh}\right]_x = 0. \quad (8)$$

One can extend the applicability of Eq. (7) to the case where instead of the specified plate temperature the heat flux $\overline{Q}_w(\overline{x})$ is imposed at the plate. The average heat flux $q_0$ is now included in the heat flux function and used as scaling for its dimensionless form $Q_w = \overline{Q}_w(\overline{x})/q_0$. The combination $q_0 h_N/k$ is then used for scaling the temperature. The corresponding boundary condition at the plate is, therefore,

$$T_z = Q_w, \quad \text{at} \quad z = 0, \quad (9)$$

that being combined with Eqs. (1) and (3), leads to the temperature distribution inside the film

$$T = \frac{Q_w}{B}[1 + B(h-z)], \quad (10)$$

from which the temperature distribution at the liquid–gas interface $z=h$ is found as

$$T_i(x) = \frac{Q_w(x)}{B}. \quad (11)$$

Equation (11) shows that the case of the adiabatic liquid–gas interface $B=0$ is singular. Using the explicit form of $T_i$ given by Eq. (11) transforms Eq. (7) into

$$h_t + Rh^2 h_x + \varepsilon\left(\frac{2}{15}R^2 h^6 h_x + S\frac{h^3}{3}h_{xxx} - M_w\frac{h^2}{2}\frac{Q_{w_x}}{B}\right)_x = 0, \quad (12)$$

where $\beta = \pi/2$ is again assumed.

In both Eqs. (12) and (8) the terms of order $\varepsilon^2$ are dropped. The two last terms of Eq. (8) show that thermocapillarity can act in two different ways. The first one is due to perturbations of the interface temperature induced by variations of $h$, when heat transfer to the gas phase takes place ($B \neq 0$). The second one is due to the nonuniformity of the heating conditions applied at the plate and, as will be shown below, can lead the liquid–gas interface to steady-state deformation. This is sometimes referred to as ''permanent deformation'' in what follows. The main purpose of this work is to investigate the effect of coupling between these two mechanisms, both arising from a nonuniformity of the interface temperature. However, it is important to note that only the second of the two above-mentioned mechanisms exists, when the heat flux is imposed at the plate. It is expressed by the last term of Eq. (12). The reason for this difference is apparent from the expressions for $T_i$, depending on $h$ in Eq. (5) and independent of $h$ in Eq. (11). Physically, it means that the long-wave thermocapillary instability is suppressed when the plate is poorly insulating. This implies boundary condition Eq. (9). In this case the temperature gradient across the layer is independent of $h$, which implies that an increase of the film thickness is accompanied by an increase of the plate temperature.

In experiments the heating is usually controlled by imposing a constant heat flux at the plate. Marchuk and Kabov[32] calculated the heat flux distribution along a local heat source and showed that it cannot be considered as constant along the plate. This nonuniformity is due to the dependence of the heat flux on the characteristics of the flow, which is found to be particularly strong when the Reynolds number is small. Therefore, in reality the present problem would probably require a mixed boundary condition. However, we use below an imposed temperature distribution at the plate and analyze only Eq. (8).

In the case of a uniform heating the last term of Eq. (8) vanishes and in front of the remaining thermocapillary term we recover the classical Marangoni number $M = \delta M_w$ based on the temperature drop across the layer $\Delta T$ instead of $\Delta T_w$. The resulting evolution equation has been extensively studied in the literature.[13,33,34]

The presence of a nonuniformity in heating will be discussed in terms of the parameter $\delta$ appearing in Eq. (8). Figure 2 shows various reference cases for a sinusoidal nonuniform temperature distribution at the plate. Note that even when $\delta=0$, Eq. (8) contains both mechanisms of thermocapillarity. Small perturbations of a uniform heating, i.e., for $\delta \gg 1$, were already studied by Van Hook *et al.*[21] in the different context for a horizontal layer only ($\beta=0$). The difference between the horizontal and inclined heated layers is profound, since in the latter the mean flow can prevent the inherent tendency of dry spot formation and allow steady-state deformations of much higher amplitude, arising from the application of a nonuniform heating. In the following we will concentrate on the case $\delta=1/2$ to illustrate the coupling between the two thermocapillary mechanisms, although other values of $\delta$ will be also used in the investigation.

## III. STATIONARY SOLUTIONS

Along with the numerical study of the spatio-temporal dynamics of the film, as described by Eq. (8) and presented in Sec. IV, we investigate stationary states of the system. In the case of a uniform heating one can find stationary solutions in the reference frame moving downstream with the phase speed of traveling waves. In the case of a nonuniform heating, the $x$-dependent temperature distribution imposed at the plate does not allow to look directly for traveling waves, because it breaks the translational invariance of the problem. Therefore, we need to split the analysis and to look for stationary solutions either in a moving reference frame with a uniform heating or in the fixed reference frame with a nonuniform heating.

### A. Moving reference frame: Uniform heating

We now search for stationary solutions of Eq. (8) in the reference frame moving downstream at a certain velocity $v$. Introducing $h(x,t) = h(\xi)$ with $\xi = x - vt$ and taking the limit $\delta \to \infty$ with $M = M_w \delta = O(1)$ corresponding to the case of a uniform heating, Eq. (8) can be integrated once to yield

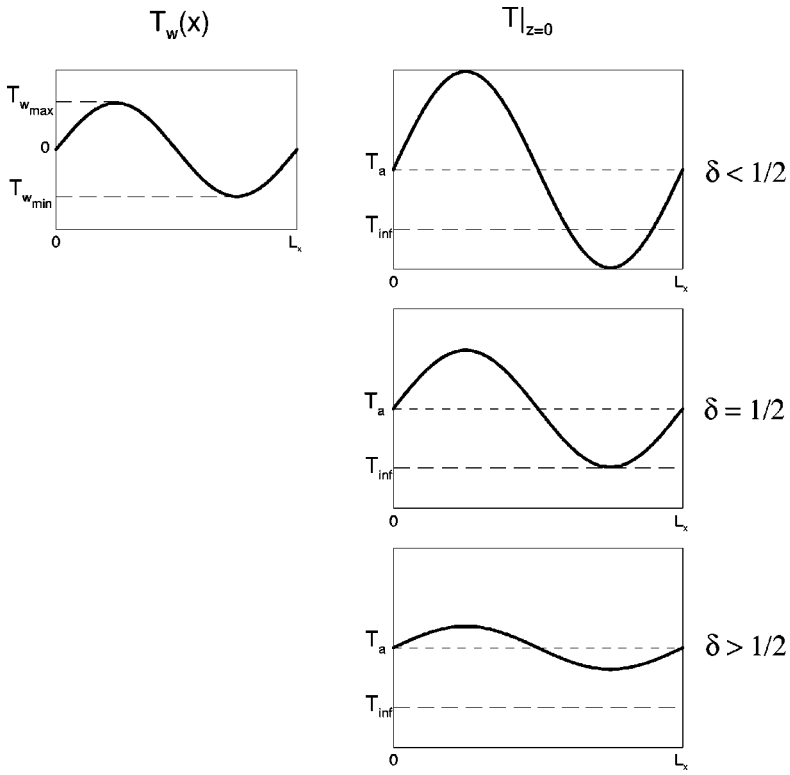


FIG. 2. On the left, a sinusoidal nonuniformity of the plate temperature $\overline{T}_w = 0.5 \sin(2\pi x/L_x)\Delta\overline{T}_w$, where $L_x$ is the length of the periodic domain. On the right, the corresponding temperature distribution applied at the plate, $\overline{T}|_{z=0} = \overline{T}_a + \overline{T}_w$, for different values of $\delta$ (the bar over the variables is omitted in the graph). When $\delta < 1/2$ (the condition should be rigorously $\delta < 1/2 - (T_{w_{\max}} + T_{w_{\min}})/2$ for nonsinusoidal temperature distribution), a section of the whole domain is cooled where the imposed temperature is lower than $\overline{T}_\infty$, while the remaining part of the domain is heated. When $\delta = 1/2$, the minimum of the imposed temperature coincides with $\overline{T}_\infty$ and the two characteristic temperature differences $\Delta\overline{T}$ and $\Delta\overline{T}_w$ are of the same order of magnitude. When $\delta > 1/2$, the intensity of the average temperature dominates that of the nonuniformity.

$$-vh + \frac{R}{3}h^3 + \varepsilon\left[\frac{2}{15}R^2h^6h_\xi + S\frac{h^3}{3}h_{\xi\xi\xi} + BM\frac{h^2}{2}\frac{h_\xi}{(1+Bh)^2}\right] = K, \tag{13}$$

where $K$ is the integration constant. The ordinary differential equation (13) can be recast into the dynamical system

$$\begin{aligned} U_1' &= U_2, \\ U_2' &= U_3, \\ U_3' &= \frac{3}{S}\left[\frac{1}{\varepsilon U_1^3}\left(vU_1 - \frac{R}{3}U_1^3 + K\right) - \frac{2}{15}R^2U_1^3U_2 - \frac{BMU_2}{2U_1(1+BU_1)^2}\right], \end{aligned} \tag{14}$$

where $U_1 = h$, $U_2 = h_\xi$, $U_3 = h_{\xi\xi}$ and prime denotes derivative with respect to $\xi$.

The solutions of the dynamical system (14) are found using the continuation and bifurcation software for ordinary differential equations AUTO 97 (Doedel *et al.*[35]). To perform the iterative search for periodic solutions for a specified set of parameters $\{\varepsilon, S, R, M, B\}$ we start with the flat film of thickness $h = 1$ (Nusselt solution) perturbed by the neutrally stable mode of the small amplitude of $10^{-3}$ with the critical wavenumber $k_c$ and the corresponding phase speed $v_c$, as obtained from the linear stability analysis[13]

$$\{k_c, v_c\} = \left\{ \sqrt{\frac{2}{5}R^2 + \frac{3BM}{2(1+B)^2}}{S}, R \right\}. \tag{15}$$

This result is easily recovered from Eq. (13) by performing a linear stability analysis of the solution $h = 1$. The starting value of the integration constant is found from Eq. (14) as $K = R/3 - v_c$. During the computations the periodicity of the solutions is enforced and the total volume is kept constant. The parameters $\{k, v, K\}$ serve as free continuation parameters into the linearly unstable domain $k < k_c$. Therefore, for any periodic solution $\mathbf{U} = \{U_1, U_2, U_3\}$, one finds corresponding values of $k$, $v$, and $K$. Even though the use of the *wavenumber* concept is rigorously correct only for harmonic modes, we prefer to associate this notion with the *period* of the domain in the case of nonharmonic modes.

As an illustration and in order to identify some reference cases for the following study, let us turn to Fig. 3, where several typical examples of stationary solutions are presented in the $[k, M]$-plane. The neutral stability curve $k_c$ given by Eq. (15) is displayed along with the wavenumber corresponding to the maximum growth rate, as given by $k = k_c/\sqrt{2}$, and with the wavenumber at which the second harmonic mode becomes linearly unstable, i.e., $k = k_c/2$. The parameter values are fixed to $R = 1.5$, $S = 5.69$, $\varepsilon = 0.1$, and $B = 0.1$ (the choice of parameters is explained in Sec. IV B). The stationary solutions are presented for the fundamental wavenumber $k_0 = \pi/10$ corresponding to the case of a periodic domain of the fixed size $L_x = 20$. By increasing $M$ one can follow the change of the shape of the solution from one hump for $M = 2.5$ [Fig. 3(a)] to two humps for $M = 20$ [Fig. 3(d)] going through the development of a secondary hump for $M = 7.5$ [Fig. 3(b)] and the coexistence between the one- and two-humped states for $M = 15$ [Fig. 3(c)]. In the latter, two stationary solutions are found: the one-humped solution obtained by continuation from a single wave of $k = k_c$, and

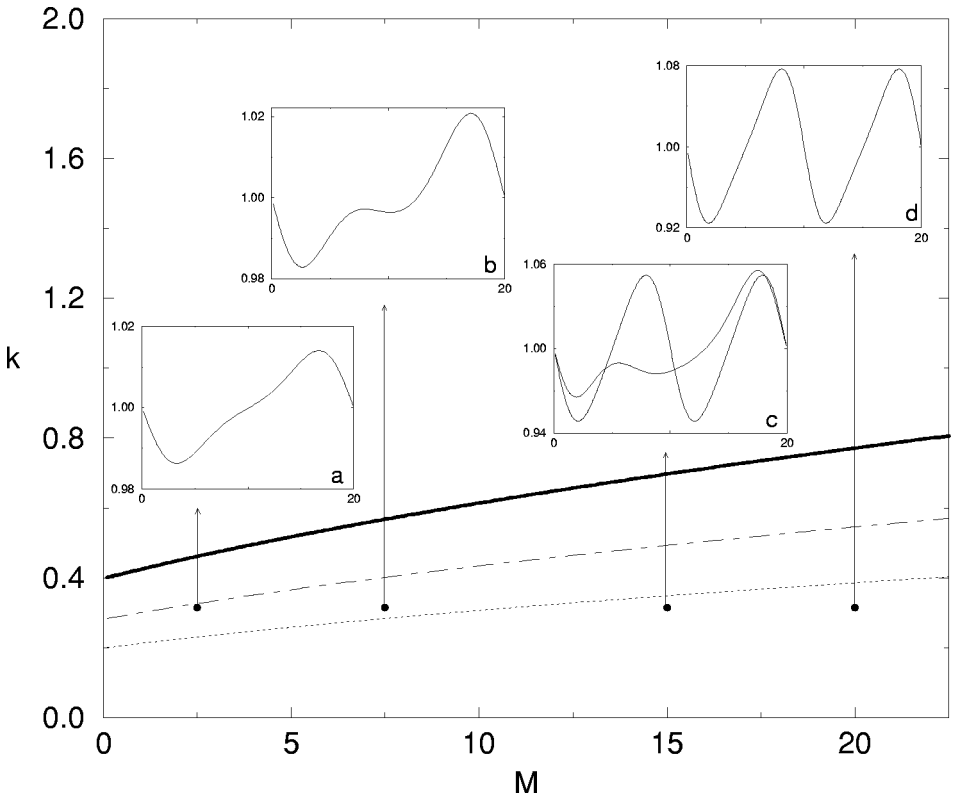


FIG. 3. Wavenumber of disturbances $k$ versus Marangoni number $M$ in the case of uniform heating for $R=1.5$, $S=5.69$, $\varepsilon=0.1$, and $B=0.1$. The thick solid line represents the cut-off wavenumber $k_c$, the dot–dashed line $k=k_c/\sqrt{2}$ represents the most amplified linear mode and the dotted line $k=k_c/2$ is the limit below which the second mode is linearly unstable. The inset figures display typical traveling waves calculated for the fundamental wavenumber $k_0=\pi/10$ and various values of the Marangoni number $M$ (a) 2.5, (b) 7.5, (c) 15, and (d) 20. The phase velocities $v$ for these solutions are, respectively, 1.5002, 1.5064, [1.4984; 1.5326] and 1.4972. Note that two steady solutions coexist at $M=15$.

the two-humped solution obtained by continuation from a double wave of $k=k_c/2$. The phase speed $v$ is seen to increase above $v_c=R$ for a single hump wave and to decrease below $v_c$ for a two-humped wave.

Figure 4 shows the wave amplitude $h_{\max}-h_{\min}$ versus $M$ for the interfacial waves with one and two humps, labeled there as "1" and "2," respectively. The slight fold of the curve "1" at $M\approx 7.3$ indicates the appearance of a secondary small amplitude hump, as shown in Fig. 3(b). The curve "2" emerges at $M=10.82$, where the second mode $k=2k_0$ loses its stability. The persistence of the solutions corresponding to the curves "1" and "2" is determined by solving the evolution equation (8), see Sec. IV. Three different regimes are identified by the three zones in Fig. 4: in zone I the thick solid line represents stable one-humped solutions, see Figs. 3(a), 3(b); in zone II for $M>13.8$ the two solution branches coexist and compete, see Fig. 3(c), while in zone III for $M>19.2$ the two-humped solution is dominant, as presented in Fig. 3(d) and shown here by the thick solid line. The transitions I–II and II–III were determined with an accuracy of $10^{-1}$. In Sec. IV we will extend the above discussion and explain in particular how the two-humped solution competes with the one-humped solution in zone II and becomes dominant in zone III.

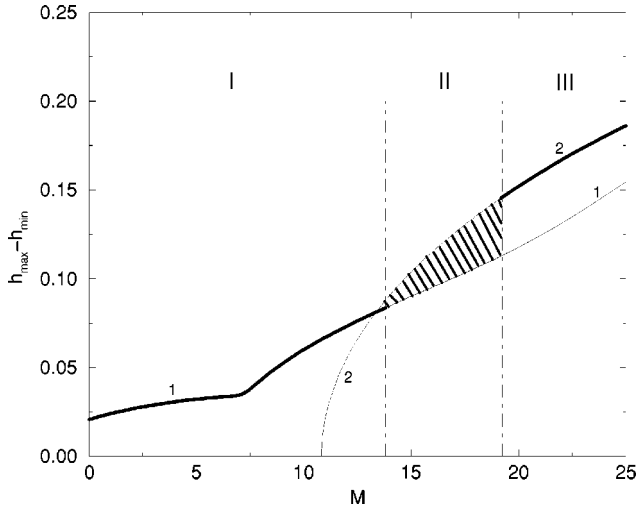


FIG. 4. Diagram displaying the wave amplitude $h_{\max}-h_{\min}$ versus the Marangoni number $M$. The parameter values used here are the same as in Fig. 3. The solid line labeled "1" corresponds to a one-humped interfacial wave with the fundamental wavenumber $k_0=\pi/10$. The solid line labeled "2" corresponds to a two-humped interfacial wave, i.e., $k_0=\pi/5$. Three zones are here delineated: in zone I the thick solid line represents the stable one-humped wave; in zone II for $M>13.8$ two solution branches coexist and compete, as illustrated by the dashed area; in zone III for $M>19.2$ the two-humped type of waves is dominant and depicted by the thick solid line.

### B. Fixed reference frame: Nonuniform heating

The dynamical system in this case is obtained by transforming Eq. (8) into the set of ordinary differential equations

$$
\begin{aligned}
U_1' &= U_2,\\
U_2' &= U_3,\\
U_3' &= \frac{3}{S}\left[\frac{1}{\varepsilon U_1^3}\left(K-\frac{R}{3}U_1^3\right)-\frac{2}{15}R^2U_1^3U_2\right.\\
&\quad\left.-\frac{BM_w(\delta+T_w)U_2}{2U_1(1+BU_1)^2}+\frac{M_wT_{w_x}}{2U_1(1+BU_1)}\right],
\end{aligned}
\tag{16}
$$

Note that prime denotes here derivative with respect to $x$. The stationary solutions of the dynamical system (16) are calculated using the same method as in Sec. III A, but now in the fixed reference frame. Therefore, they describe steady-state deformations of the liquid–gas interface. Furthermore, we start here the continuation search with a nonperturbed flat film, enforcing the boundary conditions $h=1$, $h_x \to 0$, $h_{xxx} \to 0$ and $T_w=0$, $T_{w_x} \to 0$, and determine the value of the integration constant as $K=R/3$.

We first consider a simple periodic array of heaters at the plate modeled by the sinusoidal temperature distribution

$$T_w=\frac{1}{2}\sin\left(n_w\frac{2\pi}{L_x}x\right), \tag{17}$$

where $n_w$ is the number of ''temperature waves'' imposed inside the periodic domain $L_x$. The distance along which the temperature difference $\Delta T_w$ is imposed at the plate is expressed by $L_w=L_x/2n_w$. The obtained solutions will be presented below in Sec. IV and compared to the results of the time-dependent calculations based on Eq. (8), see, for instance, Fig. 7.

## IV. TWO-DIMENSIONAL (2D) COMPUTATIONS

In this section we study the spatiotemporal dynamics of the falling liquid film, as governed by the evolution equation (8) amended with periodic temperature distribution and periodic boundary conditions in the domain $0 \leqslant x \leqslant L_x$. The cases of uniform and nonuniform heating will be separately studied in the framework of Eq. (8) and some of the results compared with those obtained in Sec. III.

The initial condition used in this investigation in the case of a uniform heating is

$$h=1+0.05\cos\left(\frac{2\pi}{L_x}x\right), \tag{18}$$

while in the case of a nonuniform heating the initial condition is chosen as

$$h=1. \tag{19}$$

In the former case stationary traveling waves are always found in the range investigated, while in the latter, either oscillatory modes or pure steady-state deformations of the film interface are observed.

### A. Numerical method

The numerical technique used here to solve the evolution equation (8) is based on the Newton–Kantorovich method, as described by Oron and Bankoff.[36] To describe the numerical method in a more compact form we choose to deal with Eq. (7) which is equivalent to Eq. (8) upon substitution of Eq. (5). Equation (7) is rewritten as

$$h_t+F(h)=0, \tag{20}$$

where

$$F(h)\equiv\left[R\frac{h^3}{3}+\varepsilon\left(\frac{2}{15}R^2h^6h_x+S\frac{h^3}{3}h_{xxx}-M_w\frac{h^2}{2}T_{i_x}\right)\right]_x.$$

Note the conservative form of Eq. (20) provided that both $T_i$ and $h$ are periodic in the given domain. Equation (20) is discretized in time using the implicit backward Euler method in the form

$$\frac{h^{(n+1)}-h^{(n)}}{\Delta t}=-F(h^{(n+1)}), \tag{21}$$

where $\Delta t$ is the time step and $h^{(n)}$ is the solution of the evolution equation obtained at the time $t_n=n\Delta t$. The right-hand side of Eq. (21) is linearized by

$$F(h^{(n+1)})=F(h^{(n)})+F_h^{(n)}(h^{(n+1)}-h^{(n)}), \tag{22}$$

where $F_h^{(n)}$ is the Frechet differential operator evaluated at the time $t_n$.

Introducing the difference between the solutions calculated for consecutive times $u\equiv h^{(n+1)}-h^{(n)}$, Eqs. (21) and (22) are combined into

$$(I+\Delta tF_h)u=-\Delta tF(h^{(n)}), \tag{23}$$

where the superscript of $F_h$ is hereafter omitted for simplicity,

$$F_hu=R(h^2u)_x+\varepsilon\left\{\frac{2}{15}R^2(h^6u_x+6h^5h_xu)_x+\frac{S}{3}(h^3u_{xxx}+3h^2uh_{xxx})_x-M_w(huT_{i_x})_x-BM_w\left[\frac{h^2}{2}\left(\frac{uT_i}{1+Bh}\right)_x\right]_x\right\},$$

$I$ is the identity operator and $T_i=T_i(x,t)$ given by Eq. (5) in the case of a specified temperature distribution at the plate. Instead, when considering a heat flux distribution at the plate, the last term of $F_hu$ will be absent. Equation (23) constitutes a linear ordinary differential equation in terms of the variable $u(x,t)$. Discretization of $F(h)$ and $F_h$ are both carried out using a central difference scheme and linear interpolation for half-nodes accurate to $O(\Delta x^2)$, where $\Delta x$ is the spatial step. $N_x$ will be the number of grid points in the spatial domain. Furthermore, the conservative forms are used in order to conserve the total volume during the computations with a sufficient accuracy. Finally, the sets of simultaneous linear algebraic equations resulting from the discretization of Eq. (23) are solved at each step directly for $u\equiv u_j$ $(j=1,\ldots N)$ using the generalized Thomas' algorithm applied to the pentadiagonal sets with three corner elements that arise due to spatial periodicity. The computations were typically performed with $N=500$ to 1000 grid points to assure spatial convergence of the solutions.

### B. Results

As already mentioned, the results are presented for the fixed parameter values of $R=1.5$, $S=5.69$, $B=0.1$, and $\varepsilon=0.1$. These values are calculated from the material properties of a 25% ethyl–alcohol solution in water given in Table I. Furthermore, we consider a moderate heat transfer coefficient of $\alpha_h=500$ W/m$^2$ K and fix the mean film thickness to $h_N=100$ $\mu$m. The chosen value of the small parameter $\varepsilon$ ensures that $S=O(1)$.

TABLE I. Fluid properties for a 25% ethyl–alcohol solution in water at 20 °C.

| | | | |
|---|---|---|---|
| $\rho$ | 961.6 | kg/m$^3$ | density |
| $\nu$ | $2.548\times10^{-6}$ | m$^2$/s | kinematic viscosity |
| $k$ | 0.4786 | W/mK | heat conductivity |
| $\sigma_\infty$ | $35.53\times10^{-3}$ | N/m | mean surface tension |
| $\gamma$ | $0.1103\times10^{-3}$ | N/mK | surface tension variation with $T$ |
| $Pr$ | 21.8 | ··· | Prandtl number |

Before using the BE as a model equation, it is crucial to estimate its range of validity. This can be made in terms of the values of the Reynolds number $R$ and the Kapitza number

$$Ka=\frac{\sigma_\infty}{\rho g^{1/3}\nu^{4/3}},$$

which represents a dimensionless measure of surface tension and depends on the liquid properties only. Just as a reference in the case of water at 20 °C, $Ka\approx3400$. Ruyer-Quil and Manneville[18] showed that a blowup of the BE takes place at $R=R^\star$ which is $R^\star\approx4.5$ for $Ka=252$, and that the maximum amplitude of a one-hump interfacial wave does not deviate more than 1% from their model, up to $R=0.9R^\star$. In the present paper, we consider a liquid with higher surface tension corresponding to $Ka=495$. For the parameter set used in most of our computations presented here, we numerically observe the blowup of the solution for Eq. (8) at $R=R^\star\approx7.5$. It is important to note here that for the same parameter set the value of $R$ corresponding to the linear stability threshold of the system is $R=R_0\approx1.185$. The main part of our investigation is carried out at $R=1.5$ that constitutes 20% of $R^\star$ and exceeding $R_0$ by approximately 25%. It thus follows that this regime is in the domain adjacent to the linear stability threshold of the system, and a use of the BE is justified.[11] The thermocapillary effect can be safely added to the isothermal case leading to Eq. (8) being valid for a study of the heated film dynamics slightly farther from the linear stability threshold.

We also note that the smaller is surface tension, the more significant is the role of the viscous dissipation on wave dynamics. This leads to a decrease of $R^\star$ with a decrease of $Ka$, and thus to shrinkage of the validity range of the BE. This was estimated quantitatively by Nguyen and Balakotaiah[38] who evaluated the influence of some viscous terms in the governing equations that are usually disregarded in other models. Following this, our study should not be extended into the domain of small values of $Ka$, such as $Ka<10$.

As mentioned above, Ruyer-Quil and Manneville[18,19] suggest that one should avoid approaching the blowup regime by a factor 0.9 to ensure the validity of the BE and the accuracy of the long-wave model. In view of the fact that the thermocapillary effects will be added to the BE we choose to keep the value of $R$ below $0.4R^\star$.

Several attempts to compare between the solutions for the Benney equation and those for the full Navier–Stokes equations are reported in the literature. Ramaswamy *et al.*[34] found an excellent agreement between those for $R=1$, $Ka=300$ when the wavenumber of the disturbance corresponds to the wavenumber of the most amplified linear mode and its first subharmonics. Salamon *et al.*[37] also reported very good agreement in the domain close to the linear stability threshold of the film. The reader is referred to the discussion in Oron and Gottlieb.[11]

The computations here are carried out for a sinusoidal temperature distribution given by Eq. (17), focusing primarily on the influence of the imposed temperature gradient by varying $M_w$ and $n_w$. Next, the influence of the average temperature on the dynamics is studied by varying the value of the parameter $\delta$. The results are compared to those obtained in the case of a uniform heating by using Eq. (8) in the limit of $\delta\to\infty$, setting $M=\delta M_w=O(1)$ and with Eq. (18) as the initial condition. We find that no noticeable differences are observed when other initial conditions, such as a random perturbation of the uniform state $h\equiv1$, are employed.

### 1. Influence of the imposed temperature gradient

In this subsection we study the film dynamics along with a sinusoidal temperature distribution at the plate given by Eq. (17). Figure 5 shows the early stage of the evolution of the film thickness in the case of one ''temperature wave,'' i.e., $n_w=1$, imposed inside the periodic domain, with $M_w=5$. The initial condition is given by the flat state, Eq. (19), which does not satisfy the evolution equation (8) due to the prescribed nonzero temperature gradient appearing in the last term. The evolution is presented over one period characterized by the time $t_c=L_x/v_c$, where $v_c$ is the phase speed of interfacial waves given by Eq. (15) and predicted by the linear theory in the case of a uniform heating.[13] The flat film is deformed first by the thermocapillary stress that induces a flow from a hotter point to a colder one. This flow creates a trough in the left half of the domain and a crest in the right half of the domain, as shown in Fig. 5(a). This deformation is advected by the flow as shown in Fig. 5(b), and grows quickly to reach its maximum at $t\approx t_c/2$, as indicated by the thick long-dashed curve. This quick increase of the amplitude occurs when the phase of the modulated traveling wave matches that of the permanent deformation. Further, the wave disintegrates into two waves and its amplitude significantly reduces until reaching its minimum at $t\approx t_c$, as shown by the thick dotted curve. One observes that the traveling wave is modulated by a well-defined envelope. The presence of this envelope is the direct consequence of the periodic temperature profile $T_{w_x}$ imposed at the plate. Figure 5(c) shows that an oscillatory regime is reached in the long time limit. Again a sequence of events of total duration $t_c$ is displayed and clearly shows the presence of the envelope.

The fixed stationary solution calculated from the dynamical system Eqs. (16) is also displayed in Fig. 5(c). It appears to be in the middle of the above-mentioned envelope, as indicated by the thick dotted curve. Figure 5(d) shows the corresponding evolution in the case of a uniform heating for $M=2.5$ ($\equiv\delta M_w$) giving rise to a traveling wave. This traveling wave was calculated as a stationary solution in the moving frame of reference from the dynamical system Eqs. (14) and is shown by the thick dotted line. The phase

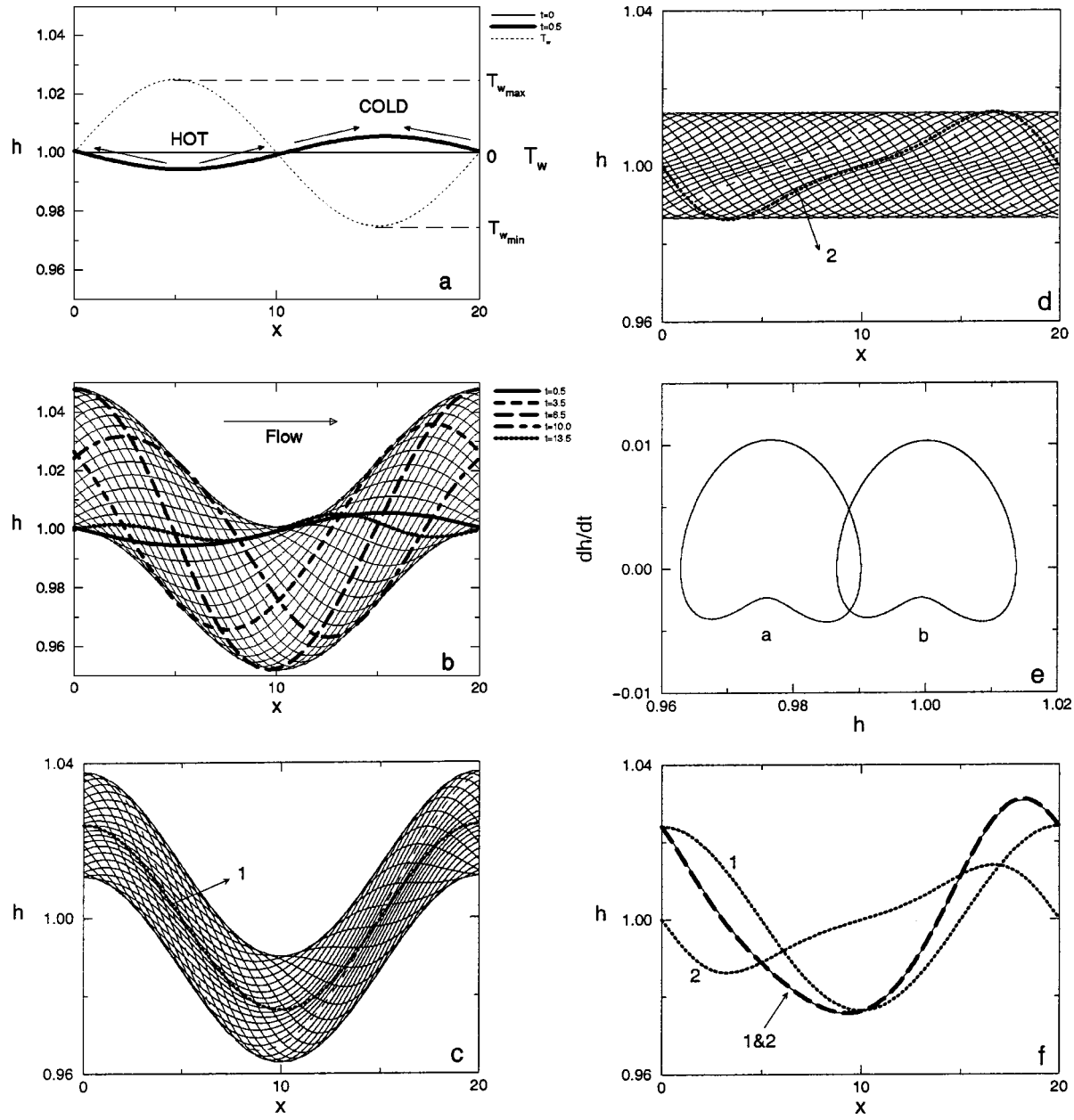


FIG. 5. Film evolution as described by Eq. (8) for $M_w=5$, $\delta=0.5$, $R=1.5$, $S=5.69$, $B=0.1$, $\varepsilon=0.1$, and $L_x=20$. (a) The initial condition at $t=0$ is a flat film $h=1$. At $t=0.5$ a depression of the liquid–gas interface emerges where the temperature is higher (HOT) than the average one, as surface tension decreases with temperature, and the elevation of the liquid–gas interface takes place where the temperature is lower (COLD). The nonuniform component $T_w(x)$ of the plate temperature is also drawn (dashed line) and scaled on the right vertical axis. (b) Evolution of the liquid–gas interface at the early stage from $t=0.5$ to $t=13.5$ shown with increments of 0.5. The deformation is advected by the flow in the direction indicated by the horizontal arrow. Five snapshots are shown by thick curves and labeled in the legend in order to allow the reader to follow the evolution of the liquid–gas interface. (c) Oscillatory mode from $t=3486.5$ (dashed line) to $t=3500$ shown with increments of 0.5. The thick dotted line marked "1" is the corresponding stationary solution calculated in the fixed reference frame. (d) Same as (c) but for a uniform plate temperature with $M=2.5$. The stationary wave shown by the thick dotted line marked "2" is calculated in the moving reference frame. (e) The evolution of the cases shown in (c) and (d) at the fixed location $x=10$ (mid-domain) projected onto the phase plane marked by "a" and "b," respectively. (f) The above-mentioned stationary solutions "1" and "2" shown by thick curves and their linear superposition labeled "1&2," as shown by the thick long-dashed line. The latter almost coincides with the computed solution for $t=3498$, as indicated by the thin solid line.

space portraits in both cases of uniform and nonuniform heating, shown in Fig. 5(e), demonstrate the similarity between the two waves and suggests that for small nonuniformities of the temperature profile, the oscillatory mode can be expressed as $h_s(x,t)\approx h_0(x)+h_{tr}(x-v_c t)$ representing a superposition of the fixed and traveling stationary waves, $h_0$ and $h_{tr}$, respectively. Figure 5(f) demonstrates an excellent agreement between the superposition of the two above-mentioned stationary waves and the corresponding computed solution at the time shown in the graph. This consideration is found to be valid for sufficiently small Marangoni number $M_w$ only.

Figure 6(a) presents the modulated wave, i.e., the oscillatory regime, obtained for $M_w=15$, $n_w=1$ and $\delta=1/2$, while Fig. 6(b) shows the corresponding case of a uniformly heated plate for $M=7.5$. The apparently thick line region in

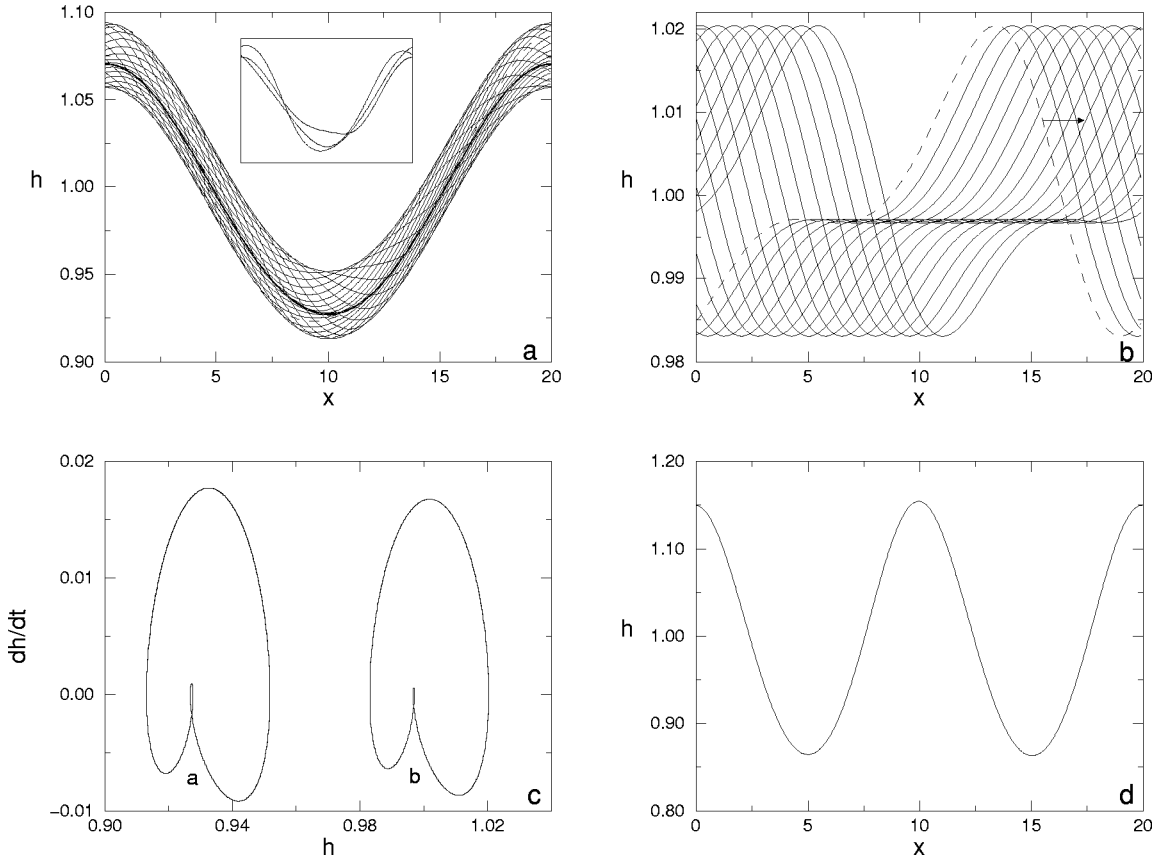


FIG. 6. The film evolution as described by Eq. (8) for $M_w=15$, $\delta=0.5$, $R=1.5$, $S=5.69$, $B=0.1$, $\varepsilon=0.1$, and $L_x=20$. (a) Film evolution from $t=3486.5$ (dashed line) to $t=3500$ shown by increments of 0.5. The apparently thick line is the locus of the secondary hump of the traveling wave modulated by the permanent deformation. Snapshots of computed waves are plotted in the inset in order to obtain a better idea of their instantaneous shape. (b) Same as (a) for the case of a uniform plate temperature with $M=7.5$. The arrow indicates the direction of propagation. (c) Phase plane portraits corresponding to (a) and (b) at the location $x=10$. (d) Same as (a) for the case of two "temperature waves," $n_w=2$. In this case the deformation of the interface is steady in time (no oscillations).

both cases is the locus of the fold between two humps already mentioned in the text, Fig. 3(b). This reflects the fact that in these conditions the wave preserves its characteristics, whatever is the temperature gradient applied at the plate, Fig. 6(b). Nevertheless, the phase space portrait shown in Fig. 6(c) now exhibits some differences which reveal the inaccuracy of the superposition of $h_0$ and $h_{tr}$. When $n_w=2$, i.e., the strength of the imposed temperature gradient is doubled, the wave becomes steady (fixed point) instead of a propagating wave (limit cycle), as shown in Fig. 6(d). This result suggests that a sufficiently strong temperature gradient along the plate can suppress the oscillatory regime and give rise to a steady-state deformation of the liquid–gas interface.

Figure 7 displays a comparison between the cases of a "frozen" liquid–gas interface obtained from numerical solution of Eq. (8) (solid line) and the stationary solution calculated in the fixed frame of reference using the dynamical system (16) (dashed line). The excellent agreement evident from Fig. 7 provides also a verification of our numerics, since the solutions were calculated by two different numerical methods.

It is found by comparing graphs in Fig. 7, that the amplitude of the emerging wave is approximately proportional to the value of the imposed temperature gradient along the plate. Indeed, in the limit of small Biot number ($B\ll 1$) and small, order $\varepsilon$, deformations of the liquid–gas interface in Eq. (8), while neglecting the effect of curvature, and for steady case ($h_t=0$) we find the following approximation for the film thickness by neglecting the terms of order $\varepsilon^2$:

$$h\approx 1+\varepsilon\frac{M_w}{2R}T_{w_x}=1+\varepsilon\frac{M_w}{2R}n_w\frac{\pi}{L_x}\cos\left(n_w\frac{2\pi}{L_x}x\right), \quad (24)$$

when using Eq. (17) for the temperature distribution $T_w$. Nevertheless, even though the value of $M_w$ is about twice higher in Fig. 7(e) than in Fig. 7(d), the departure from the sinusoidal shape is observed through the slight asymmetry of the troughs being a manifestation of nonlinearities.

Figure 8 presents the film evolution for $M_w=40$ that corresponds to the case of a uniform heating with $M=20$ ($M_w=\delta M$) belonging to zone III of Fig. 4. Hence the emergence of a two-humped wave is expected, as shown in Fig. 8(b). This two-humped wave persists when the plate temperature is nonuniform [Fig. 8(a)]. However, the phase velocity slightly decreases by 1.3% with respect to the case of a uniform heating, so the presence of the permanent deformation induces a slowdown of the wave propagation. This effect is even more pronounced for larger temperature gradi-

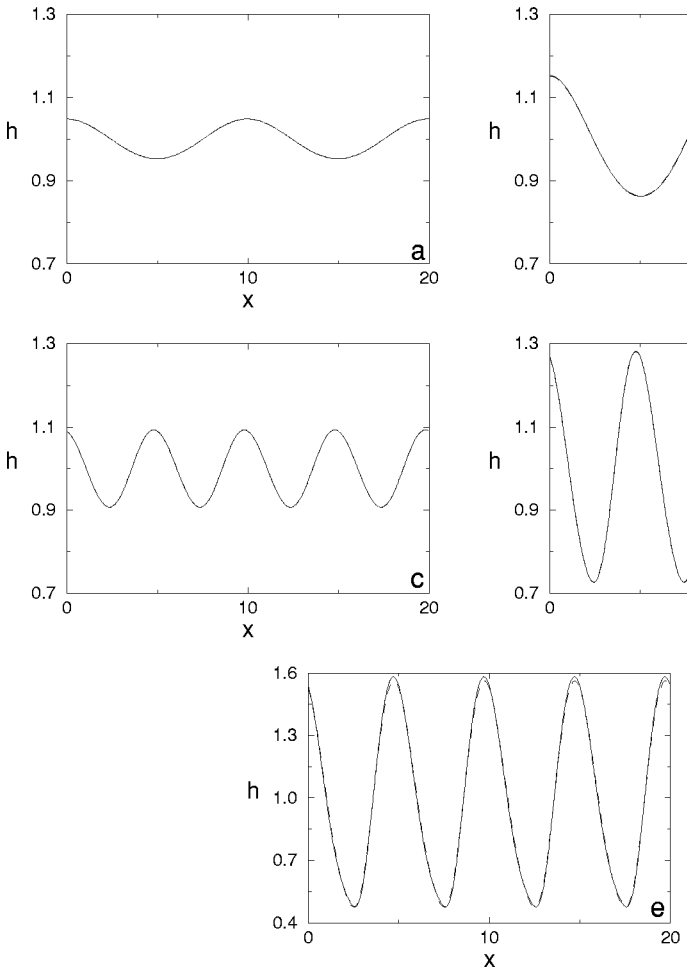


FIG. 7. Stationary solutions obtained from numerical solution of Eq. (8) (solid lines) and calculated in the fixed frame of reference from the dynamical system (16) (dashed line). The parameter values are $\delta=0.5$, $R=1.5$, $S=5.69$, $\varepsilon=0.1$ and $B=0.1$. (a) $M_w=5$ and $n_w=2$; (b) $M_w=15$ and $n_w=2$; (c) $M_w=5$ and $n_w=4$; (d) $M_w=15$ and $n_w=4$; (e) $M_w=30$ and $n_w=4$. The differences between the solid and dashed curves are observable only in the case (e), where the temperature gradient is the largest.

ents, for instance a decrease of 5.3% when $n_w=2$, see Fig. 8(c). Finally, the propagation becomes aperiodic when $n_w=4$ [Fig. 8(d)]. These evolutions are summarized in the phase plane portraits presented in Fig. 8(e).

The time series of the film thickness recorded in the middle of the periodic domain $x=10$ are plotted in Figs. 9(a) and 9(c) and correspond to the cases presented in Fig. 6 for $M_w=15$ and Fig. 8 for $M_w=40$, respectively. These cases belong to zones I and III in Fig. 4. The time series are marked by the value of temperature waves $n_w$ and by "0" for the case of a uniform heating on the right side of each plot. Figure 9(b) shows the modulated time series for $M_w=30$ corresponding to zone II in Fig. 4, where the liquid–gas interface oscillates between two competing states with different fundamental frequencies. This modulation is sustained for a uniform heating and for $n_w=1$, while for $n_w=2$ the two-humped wave is dominant. In the case of $n_w=4$ the wavy dynamics of the liquid–gas interface is even suppressed giving rise to a steady-state deformation.

### 2. Influence of the average temperature

We now turn to the investigation of the influence of the average plate temperature on the film evolution in the presence of a specified plate temperature nonuniformity. Figure 10 displays the envelopes of the surface oscillations and the corresponding time series for various values of $\delta$ (recall that $\delta$ is the ratio between the temperature drop across the layer and that along the solid plate). The nonuniformity of the plate temperature is fixed in a way that $M_w=15$. In Fig. 10(a) the amplitude of the envelope for $n_w=1$ is found to increase by a factor of 3 when $\delta$ increases from $\delta=0.16$ (dotted line) to $\delta=1$ (dashed line) and by a factor of 7 when $\delta$ increases from $\delta=0.16$ to $\delta=2$ (solid line). Nevertheless, even for a large average temperature the shape of the steady-state deformation of the liquid–gas interface is determined by that of the stationary wave calculated in the fixed reference frame, and shown by the thick dot–dashed curve. The corresponding time series of the film thickness recorded at the location $x=10$ for the oscillatory regime are superposed in Fig. 10(b) and shifted, one with respect to another, for clarity.

Figure 10(b) enables us to follow the transition from a one-humped to a two-humped modulated wave with an increase of the value of $\delta$, as explained in Sec. III A. When the value of $n_w$ is doubled [Fig. 10(c)] we observe that small average temperature ($\delta=0.16$) is sufficient to sustain the steady-state deformation and the interface does not oscillate, as shown in Fig. 10(d). The same is observed in Figs. 10(e), 10(f) for $n_w=4$, in this case even for a higher average temperature of the plate ($\delta=1$). The evolution of the interface for $\delta=2$ becomes aperiodic due to strong nonlinearities involved in the dynamics, as described by Eq. (8).

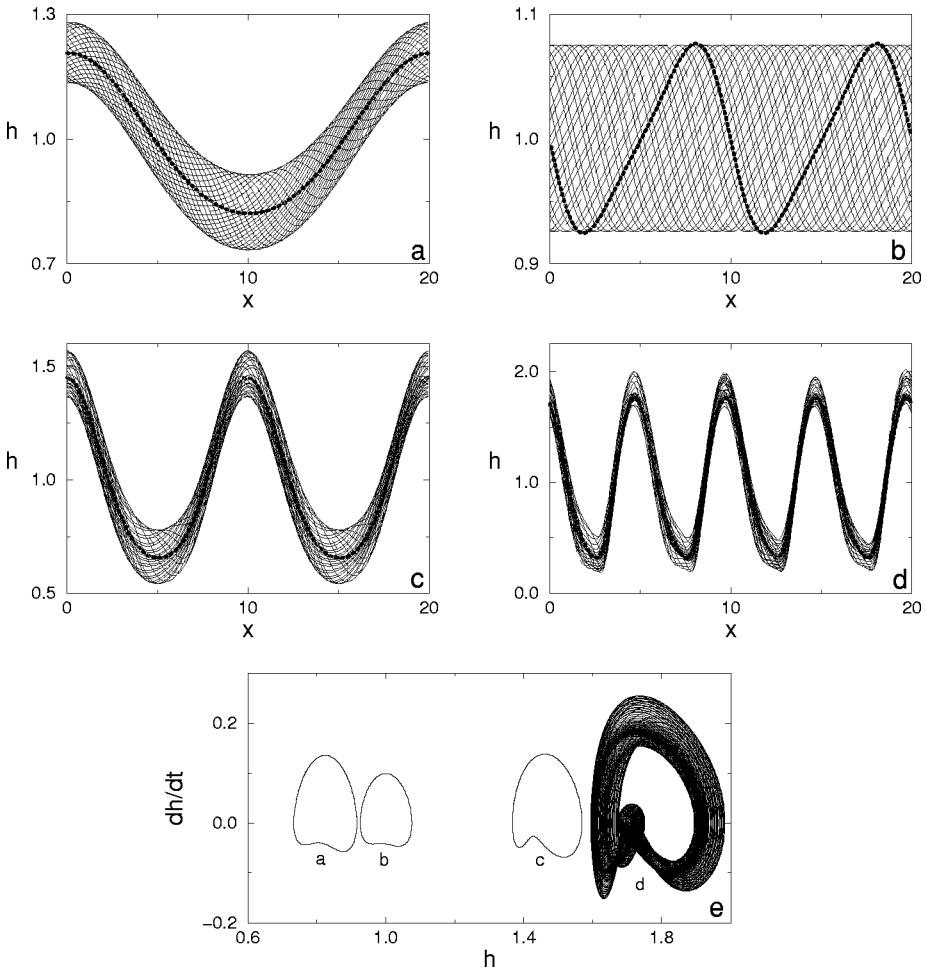


FIG. 8. The film evolution as described by Eq. (8) for $M_w=40$, $\delta=0.5$, $R=1.5$, $S=5.69$, $\varepsilon=0.1$, and $B=0.1$. (a) Film evolution from $t=3486.5$ (dashed line) to $t=3500$ shown by increments of 0.5. The thick dotted line indicates the corresponding stationary solution calculated in the fixed reference frame. (b) Same as (a) for the case of the uniform plate temperature with $M=20$. (c) Same as (a) for the case of two "temperature waves" $n_w=2$. (d) Same as (a) for the case of four "temperature waves" $n_w=4$. (e) Phase plane portraits corresponding to (a)–(d) at $x=10$.

## V. HEAT TRANSFER

One of the practical interests in this study is to evaluate a possible enhancement of the heat transfer coefficient due to free-surface deformations. The definition of this coefficient in its dimensionless form is chosen to be based on the temperature difference between the plate and the interface, so that using either Eq. (4) or Eq. (10) for the temperature field, the local heat transfer coefficient is

$$\hat{\alpha}(x,t)=\frac{-\left.\dfrac{\partial T}{\partial z}\right|_{z=0}}{T|_{z=0}-T_i}=\frac{1}{h(x,t)}, \tag{25}$$

and the average heat transfer coefficient computed over the periodic domain $L_x$ reads

$$\alpha=\frac{1}{L_x}\int_0^{L_x}\frac{1}{h}dx. \tag{26}$$

This result, obtained for both thermal boundary conditions at the plate, suggests that the heat transfer is inversely proportional to the film thickness. Moreover, it also shows that the free-surface deformation is not a sufficient condition for the enhancement of the heat transfer. To achieve such an enhancement the deformation must induce a sufficiently large range of thinning.

Figure 11 presents the average heat transfer coefficient given by Eq. (26) for the stationary solutions calculated in the fixed reference frame using the dynamical system (16), with the temperature distribution at the plate Eq. (17) for $n_w=1,2$ and 4. The heat transfer coefficient $\alpha$ is found to be 25% higher for $n_w=4$ than for $n_w=1$ or 2. We also present the same result for a pure sinusoidal liquid–gas interface (dot–dashed line). It appears that the deviation from the sinusoidal shape strongly diminishes the influence on variation of the heat transfer coefficient with traveling wave amplitude.

Figure 12 displays the average heat transfer coefficient plotted against the ratio $M_w/L_w$ which represents an appropriate parameter to examine the effect of the imposed temperature gradient. In Fig. 12 we also present the results obtained from the numerical solution of Eq. (8). As shown in Sec. IV, the numerical solution of Eq. (8) reveals among others oscillatory regimes in the form of traveling waves modulated by the permanent deformation. The average heat transfer coefficient of these regimes is only slightly enhanced due to the oscillatory nature of the liquid–gas interface. Nevertheless, we can conclude here that the fixed stationary solution appears to give a good estimate of the heat transfer coefficient even when the oscillatory regime takes place.

In Fig. 13 the average heat transfer coefficient is shown

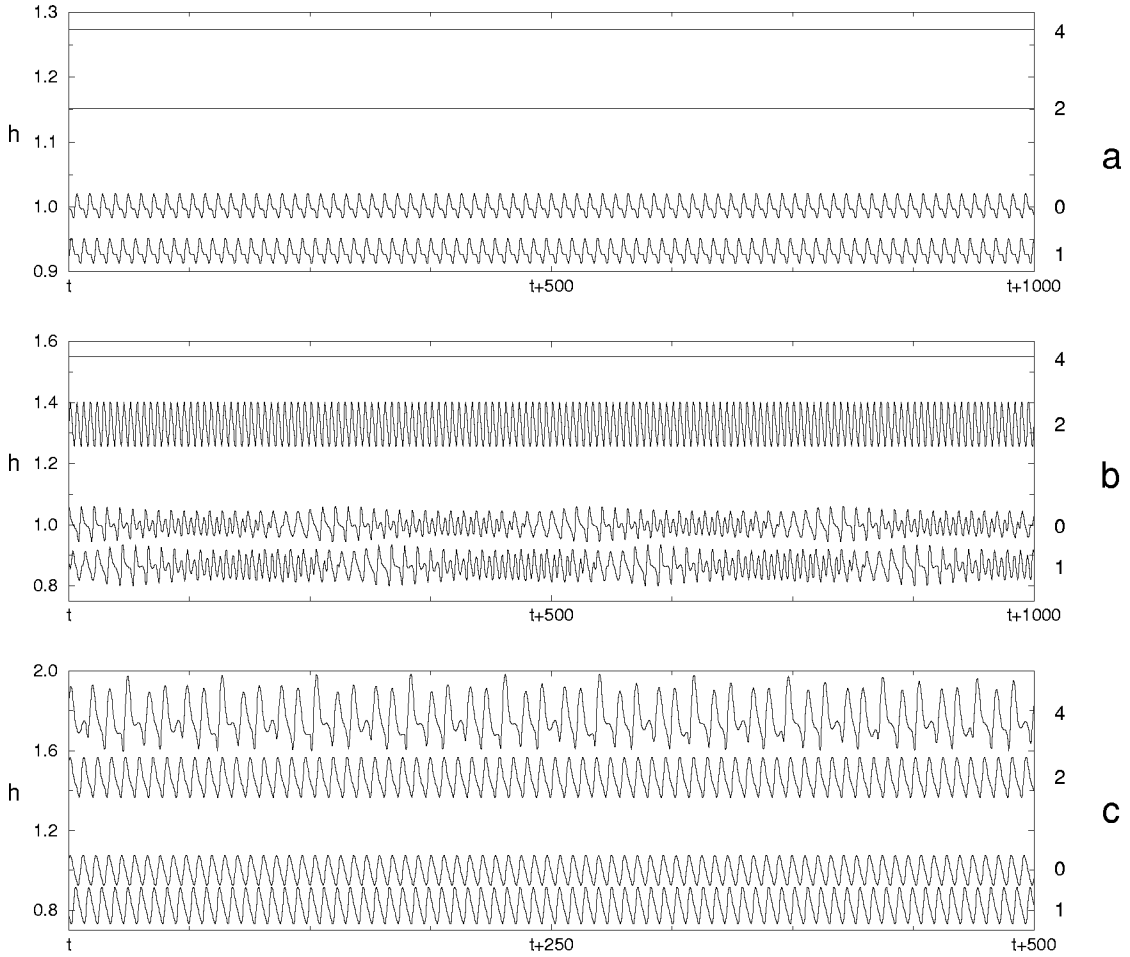


FIG. 9. Time series of the film thickness at $x=10$ for $\delta=0.5$, $R=1.5$, $S=5.69$, $B=0.1$, $\varepsilon=0.1$, $L_x=20$. On the right side of each plot the value of $n_w$ $(=0,1,2,4)$ is displayed. Here $n_w=0$ corresponds to the case of the uniform plate temperature. The corresponding Marangoni numbers are (a) $M_w=15$, (b) $M_w=30$, and (c) $M_w=40$.

as a function of the average temperature $\delta$. The white symbols correspond to the cases studied in Fig. 10 when $M_w=15$ and the black ones when $M_w=30$. It appears that the value of $\delta$ does not significantly affect the heat transfer coefficient, except for very strong temperature gradients imposed at the plate, such as for $M_w=30$ and $n_w=4$. We can conclude, therefore, that permanent deformations induced by a nonuniform heating are the main agent of heat transfer enhancement, while the amplitude of traveling waves depending on the average plate temperature does not play a significant role, as already noted in Fig. 12.

Finally, we note that in some works, see for instance Marchuk *et al.*,[32] the heat transfer coefficient is based on a mean-weighted with the local velocity temperature of the liquid film, rather than on the interface temperature $T_i$. However, we found that this alternative definition is proportional by a factor of $1.6\pm10^{-2}$ to that calculated using Eq. (25).

## VI. COMPARISON WITH EXPERIMENTS

In this section we attempt to compare stationary solutions calculated in the fixed reference frame to available experimental data.[26] We also perform some more time-dependent computations of the corresponding cases in order to complete the comparison.

Recent experiments performed on falling liquid films with localized heating[26] were focused on the measurements of the film thickness profile in the flow direction. It was found[26,27] that if the temperature gradient is aligned with the flow at the upper edge of the heater, the thermocapillary flow directed in the opposite direction deforms the liquid–gas interface into a horizontal bump, as illustrated in Fig. 14.

Since the exact temperature distribution at the plate is unknown, we use an approximate step function

$$T_w(x)=0.5\left[\tanh\left(\frac{L_x}{L_w}(x-0.25)\right)-\tanh\left(\frac{1}{0.75}(x-0.625)-1\right)\right], \tag{27}$$

to model a strong positive temperature gradient at the upper edge of the localized heater, applied along the length $L_w \ll L_x$, and centered at the first quarter of the domain $L_x$. Since the periodic boundary conditions are imposed for numerical computations, the condition $T_w(0)=T_w(L_x)$ must be

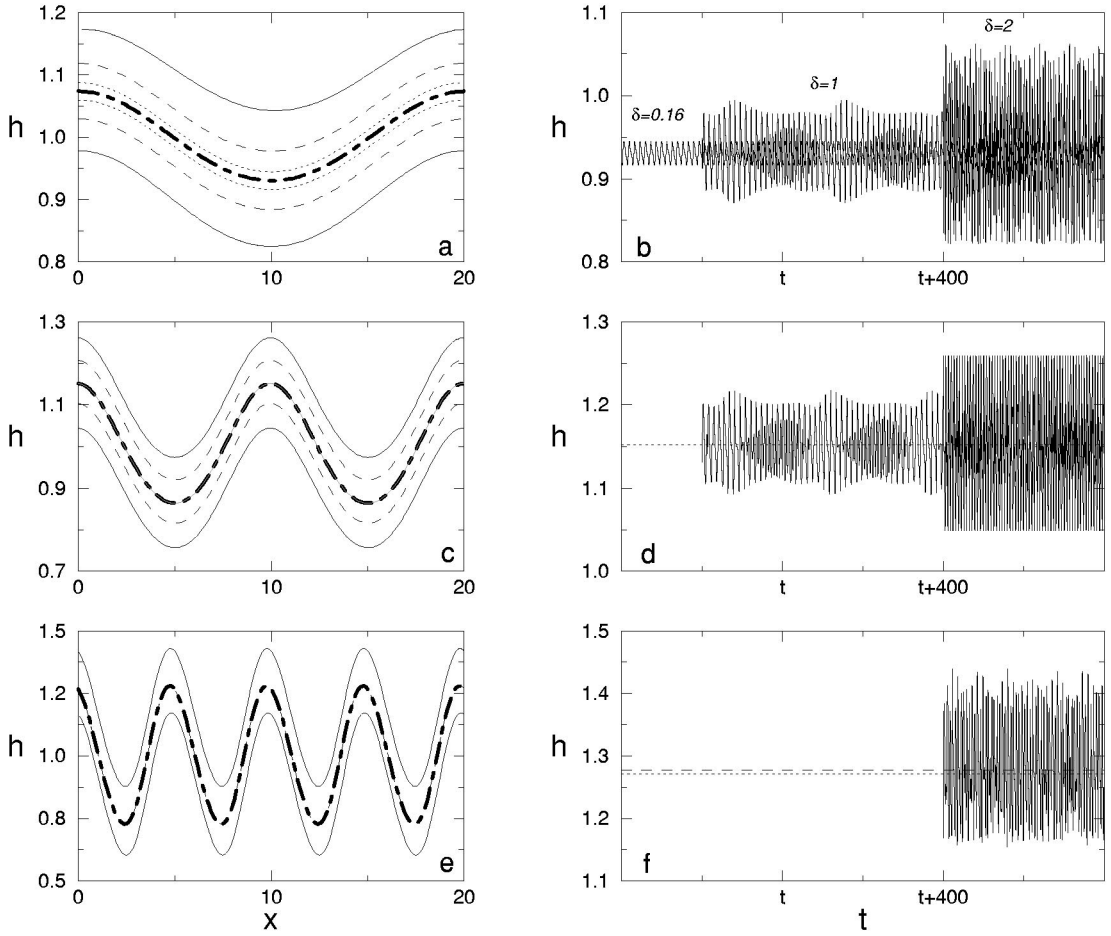


FIG. 10. The envelopes and time series of the film thickness calculated for $M_w=15$: (a) and (b) $n_w=1$; (c) and (d) $n_w=2$; (e) and (f) $n_w=4$. In the left column the dotted, dashed, and solid curves correspond to the envelopes for $\delta=0.16$, $\delta=1$, and $\delta=2$, respectively. The thick dot-dashed curves depict the corresponding steady-state solutions calculated in the fixed frame of reference. In the right column the corresponding time series recorded at $x=10$ are shifted one with respect to another for clarity.

satisfied. Moreover, the experiments showed that the interfacial temperature decreases slowly downstream due to the insulating feature of the plate where the localized heater is embedded. This is the reason why Eq. (27) features a smooth negative temperature gradient along the interval equal to 75% of $L_x$ and centered at 5/8 of the latter. Therefore, the negative temperature gradient decreases with increase of the size of the periodic domain $L_x$. One then expects that for sufficiently large $L_x$ the temperature profile tends to that of the experimental conditions. Figure 15 displays an example of the temperature distribution given by Eq. (27) for $L_x=20$ and $L_w=1$.

Figure 16 presents some profiles of the film thickness measured in the experiments[26] along with the stationary solutions calculated using Eqs. (16) for the temperature distribution specified by Eq. (27). The reader is referred to the work of Skotheim *et al.*[30] for linear stability of such stationary solutions. The experiments[26,29] were carried out for various values of the Reynolds number $R$, corresponding to different values of the mean film thickness $h_N$. Consequently, the values of the Biot number and of the surface tension number, as well as of $\varepsilon$, differ from those used above in this work. The specific value of the Marangoni number $M_{w_c}$ is-calculated to obtain a bump profile with the same maximal

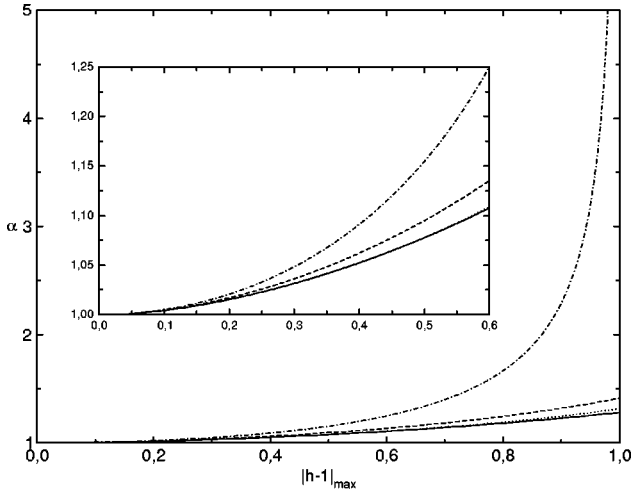


FIG. 11. Average heat transfer coefficient $\alpha$ versus the maximal deviation of the film thickness from the state $h=1$. The curves are obtained from the dynamical system Eq. (16) by increasing $M_w$ from 0 until reaching $|h-1|_{\max}=1$. The solid, dotted and dashed lines are calculated for the stationary solutions in the fixed reference frame for the sinusoidal temperature distribution with $n_w=1,2$ and 4, respectively. The parameter values are $\delta=0.5$, $R=1.5$, $S=5.69$, $B=0.1$, $\varepsilon=0.1$, and $L_x=20$. The dot–dashed line corresponds to the case of a sinusoidal shape of the liquid–gas interface. The inset is a zoom of the domain of small values of $\alpha$. Note that the dotted curve almost coincides with the solid one.

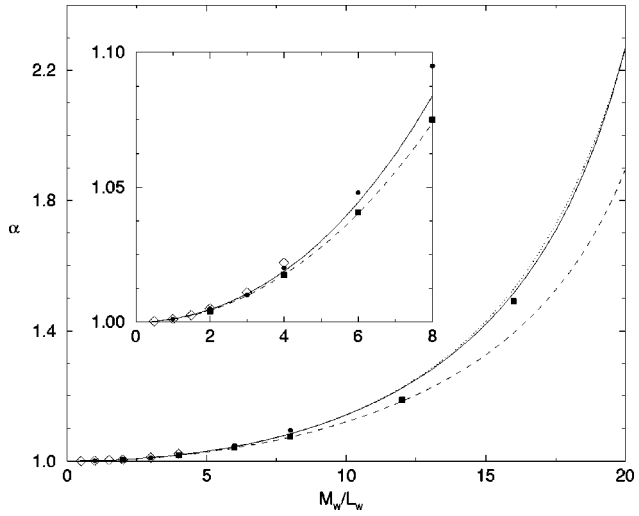


FIG. 12. Average heat transfer coefficient for stationary solutions versus the ratio between the Marangoni number $M_w$ and the distance $L_w$ $(=L_x/2n_w)$ along which the temperature difference $\Delta T_w$ is imposed at the plate. The parameter values are $\delta=0.5$, $R=1.5$, $S=5.69$, $B=0.1$, $\varepsilon=0.1$, and $L_x=20$. The curves correspond to the stationary solutions calculated in the fixed reference frame, while the symbols correspond to the related oscillatory regimes obtained by numerical simulation (see Sec. IV). The results shown are for $n_w=1$ (solid line and diamond), $n_w=2$ (dotted line and black circle) and $n_w=4$ (dashed line and black square).

film thickness as in the experiments at the instability onset of the bump. Indeed, beyond this threshold the horizontal bump breaks into longitudinal rivulets.[26] The temperature difference is then checked and is of order 10 K which agrees with the experimental data[27] and validates the choice of the parameter $\varepsilon$. Figure 16 shows that the calculated shape of the bump fits well the experimentally measured one, at least as far as its ascending side and the small depression upstream due to the surface tension effect are concerned. The discrepancy observed downstream can be attributed not only to the accumulating error associated with the integration method

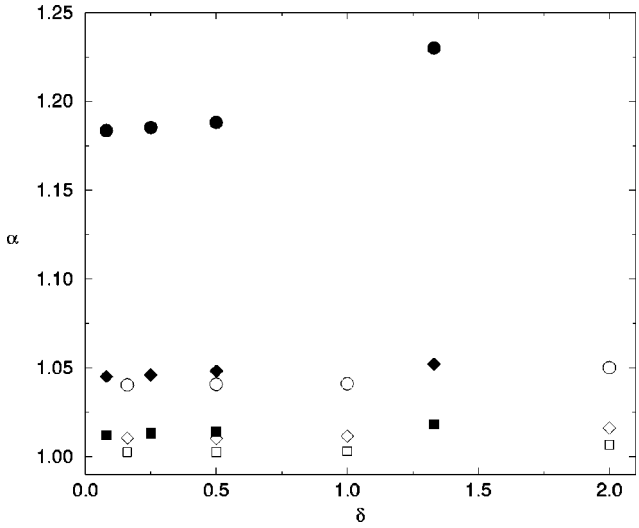


FIG. 13. Average heat transfer coefficient as a function of the parameter $\delta$ for $R=1.5$, $S=5.69$, $B=0.1$, $\varepsilon=0.1$, and $L_x=20$. The white symbols denote the results for $M_w=15$, while the black ones correspond to $M_w=30$. The squares correspond to $n_w=1$, the diamonds to $n_w=2$ and the circles to $n_w=4$.

used in processing of the experimental data, but also to the absence of temperature-dependence of the viscosity in our theoretical model. The latter effect considered by Kabov *et al.*[29] can indeed explain the decrease of the film thickness below its initial mean value $h_N$. In fact, liquid viscosity decreases when temperature increases, and as the fluid becomes more mobile, its velocity increases. Therefore, due to the flow rate conservation the film thickness indeed decreases.

Figure 17 shows the maximal deflection of the liquid–gas interface $h_{\max}-1$ as a function of the Marangoni number $M_w$. The amplitude of the deformation decreases with increase of $R$ when $M_w$ is fixed. This is the effect of the main flow that counteracts the thermocapillary flow. Similarly, the amplitude of the critical temperature difference as described by $M_{w_c}$ could be expected to increase with $R$. Nevertheless, this is incorrect, as it can be seen in Fig. 17 for $1.5 \leqslant R \leqslant 3$. An explanation is obtained on the basis of the energy balance considerations made recently by Skotheim *et al.*[30] They found that the presence of a bump deformation is stabilizing. It follows from here that the higher is the bump, the larger $M_w$ should be to allow the spanwise thermocapillary mode to develop. Therefore, with an increase of $R$ the main flow counteracts the increase of the bump amplitude. Thus the critical value of $M_w$ does not necessarily increase with $R$. This can explain why above a certain value of the Reynolds number, namely $R \approx 1$, the value of $M_{w_c}$ varies only slightly with $R$.

In order to complete the analysis, we solve numerically Eq. (8) to simulate the dynamics of the falling film with the imposed temperature distribution specified by Eq. (27). Figure 18(a) shows the propagation of the interfacial wave in the positive $x$-direction being squeezed into a steady envelope, as already observed in Sec. IV. In Fig. 18(b) we show the time series of the film thickness at $x=L_x/4$ and $x=L_x/2$. It appears that asymmetric temperature distribution does not significantly affect the dynamics of the wavy liquid–gas interface with respect to the location in the domain. In fact, Fig. 18(b) reveals an aperiodic behavior of the liquid–gas interface. The results of similar computations for $R=3$ are presented in Figs. 18(c) and 18(d). The wave amplitude is lower than for $R=1.5$ strongly influencing the heat transfer coefficient, which is approximately 1.15 for $R=1.5$ and 1.45 for $R=3$. In both cases this heat transfer enhancement is easily explained by invoking the mass conservation that thins the film in a large part of the domain, while a small portion of the fluid is driven by thermocapillarity into the bump. Indeed, we have seen in Sec. V that film thinning is favorable to heat transfer enhancement.

In both cases $R=1.5$ and 3 the wavy behavior of the liquid–gas interface observed in the numerical simulations, as well as in the experiments, can explain in a more appropriate way than previously, the discrepancies between the instantaneous measured film profiles and those calculated as stationary solutions shown in Fig. 16.

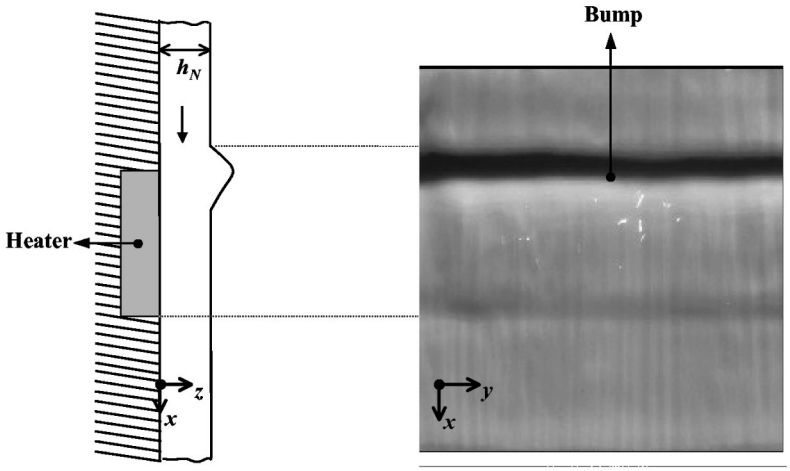


FIG. 14. The sketch on the left shows the cross section of the falling film with the mean film thickness $h_N$. The first deformation due to thermocapillarity appears at the upper edge of the localized heater and represents a horizontal bump. The front view of this bump is shown on the right. The image is obtained by optical Schlieren technique, where the positive slope in the downstream direction is seen as dark, while the negative one as bright. The coordinate system $(x,y,z)$ is also shown.

## VII. SUMMARY AND CONCLUDING REMARKS

The present theoretical investigation focuses on the study of nonlinear dynamics of a thin liquid film falling down a vertical plate with a nonuniform heating. Based on the long-wave theory we have derived an evolution equation which incorporates this heating nonuniformity and studied it. Two independent kinds of thermocapillary effects affecting the film dynamics are identified. The first one is due to perturbations of the temperature at the liquid–gas interface induced by perturbations of the film thickness in the presence of heat transfer to the gas phase, as described by a nonzero Biot number. The second one is due to the nonuniform heating of the plate. While the former is known to lead to interfacial waves, the latter is found here to be able to induce steady-state deformations of the gas–liquid interface. The relative importance of these effects is measured by the parameter $\delta$ that constitutes the ratio between the characteristic temperature differences across the liquid layer and along the plate. The value of $\delta$ is found to play an important role in the film dynamics. The coupling between these two thermocapillary mechanisms is studied here when they are comparable, i.e., $\delta = O(1)$.

Using a continuation method we have calculated stationary solutions for the pertinent evolution equation and obtained traveling waves and steady-state deformations in the cases of uniform and nonuniform heating, respectively. On one hand, the dependence of the traveling waves on the value of the Marangoni number $M$ for a pure uniform heating is studied and classified in terms of the dynamics of these waves, namely single, modulated and double waves. On the other hand, numerical solution of the evolution equation shows that the traveling wave obtained with a uniform heating is modulated by an envelope given by the steady-state deformation resulting from a nonuniform heating. At moderate Marangoni number $M_w$ the traveling wave calculated for the case of a uniform heating with $M = \delta M_w$ displays the same dynamics and the final oscillating regime represents the superposition of the fixed and stationary traveling waves. The departure from this state increases with the increase of the temperature gradient applied along the plate, until the shape of the liquid–gas interface eventually becomes ''frozen,'' thus suppressing the waves traveling along the stationary structures. A detailed study of this transition varying with the system parameters $\delta$ and the dimensionless temperature gradient along the plate $M_w/L_w$ is the subject of future work.

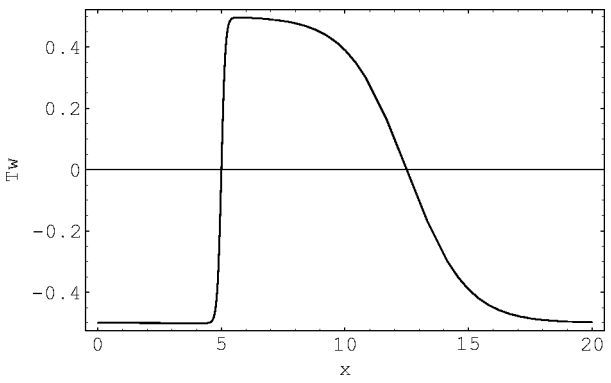


FIG. 15. A nonuniform temperature distribution $T_w(x)$, as described by Eq. (27). The length of the domain is $L_x = 20$ and the length of the positive temperature gradient is $L_w = 1$. Note that the plate temperature is $T(z=0) = \delta + T_w(x)$ with $\delta = 1/2$.

We have also assessed the enhancement of the heat transfer due to the emergence of sustained deformations and traveling waves. The latter have no significant effect on the heat transfer coefficient, while the former can increase it significantly. This holds for a sinusoidal temperature distribution, but becomes even more pronounced for a step-function temperature profile of the plate. In fact, the latter induces a localized bump that draws the liquid underneath its crest. The remaining portion of the film becomes thus thinner causing by this an increase of the local heat transfer coefficient which is proportional to the inverse of the film thickness. The evidence of quantitative improvement of the heat transfer is demonstrated here.

We have presented an analysis of a representative experimental situation using our theoretical model. The available measurements of two-dimensional film profiles are compared with the calculated periodic stationary solutions. The agreement is conclusive and allows us to proceed in the future with the three-dimensional analysis. Nevertheless, some discrepancies remain in the downstream side of the film

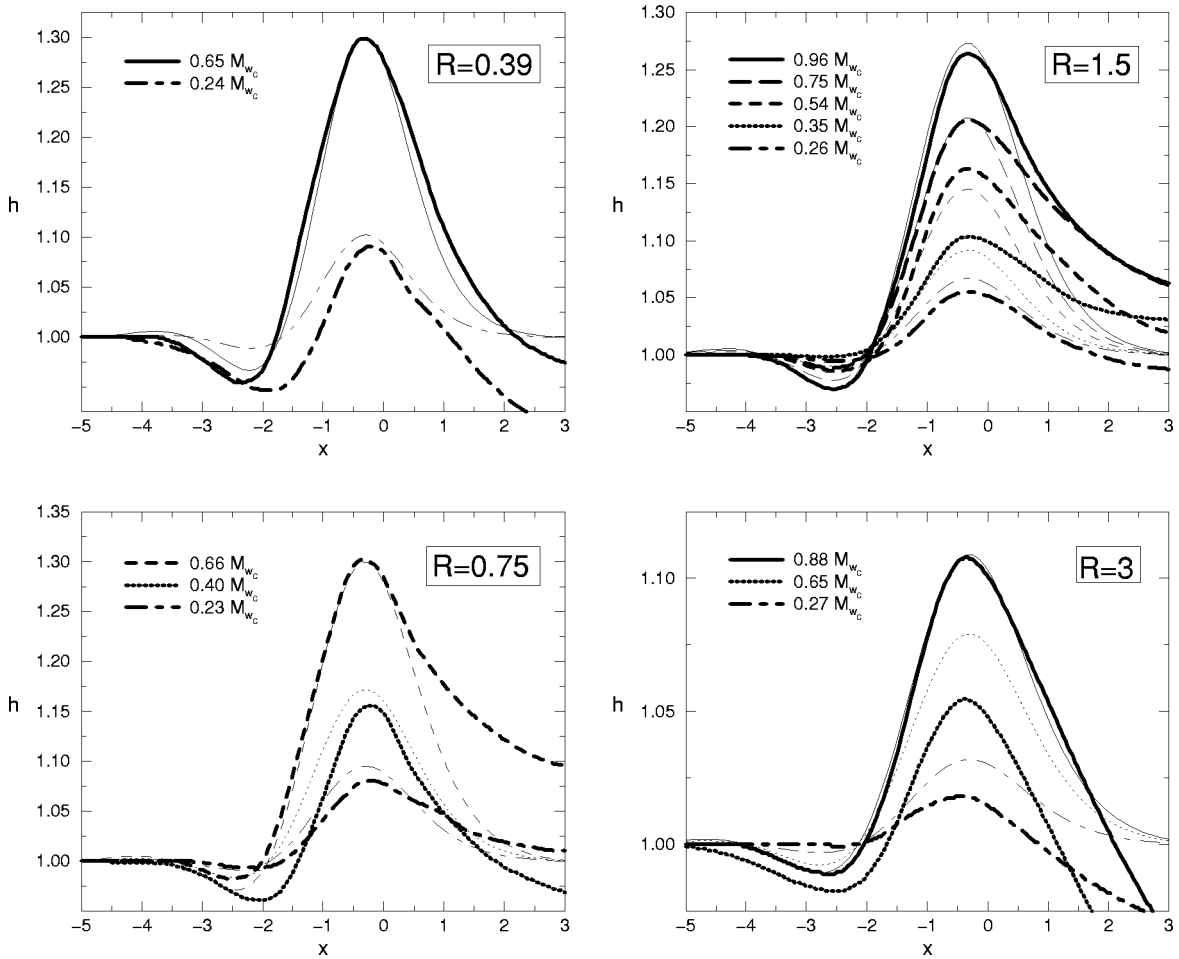


FIG. 16. Comparison between the profiles of the film thickness measured in the experiments (thick lines), and calculated from Eqs. (16) (thin lines). Each graph corresponds to a fixed value of the Reynolds number $R$. In the cases of $R=0.39,0.75,1.5,3$ the parameter sets are, respectively, $S=1.49$, $B=0.07$, $\varepsilon=0.064$, $M_{w_c}=8.5$, $L_w=4$; $S=2.8$, $B=0.08$, $\varepsilon=0.079$, $M_{w_c}=15.2$, $L_w=5$; $S=5.69$, $B=0.1$, $\varepsilon=0.1$, $M_{w_c}=16$, $L_w=5$; and $S=11.4$, $B=0.13$, $\varepsilon=0.126$, $M_{w_c}=14$, $L_w=6$. In all cases $\delta=0.5$. $M_{w_c}$ is the critical Marangoni number calculated to obtain a bump profile with the same maximal film thickness as in the experiments at the instability onset of the bump.

profiles and can be attributed either to the accumulating error, inherent to the integrating method used in the processing of the experimental data, to the absence of the temperature-dependence of liquid viscosity in the theoretical model, or, finally, to the wavy behavior of the liquid–gas interface observed in both the experiments and the theory.

In conclusion, our results can be very useful and of a practical interest in the case of strong inhomogeneity of the plate heating. Moreover, in this study we see a good starting point for future extensions into three-dimensional studies showing a great wealth of emerging dissipative structures.

## ACKNOWLEDGMENTS

The authors gratefully acknowledge fruitful discussions with Professor Oleg Kabov and Jan Skotheim. B.S. acknowledges the Technion-Israel Institute of Technology for hospitality during the visit there that became possible under the auspices of the ICOPAC Research Training Network of the European Union (Contract No. HPRN-CT-2000-00136). The research was also partially supported by the INCO-COPERNICUS program of the European Union under Grant No. ERB IC15-CT98-0908, the Deutsche Forschungsge-

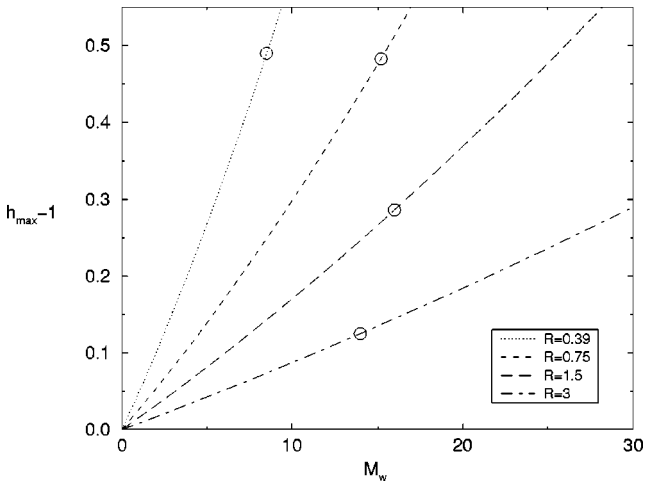


FIG. 17. Maximal departure of the liquid–gas interface from its mean dimensionless value of $h=1$ as a function of the Marangoni number $M_w$ for various values of the Reynolds number $R$. Circles represent the experimental results corresponding to the instability onset of the bump. The values of the Marangoni number at these points are the critical values denoted $M_{w_c}$, as given in Fig. 16.

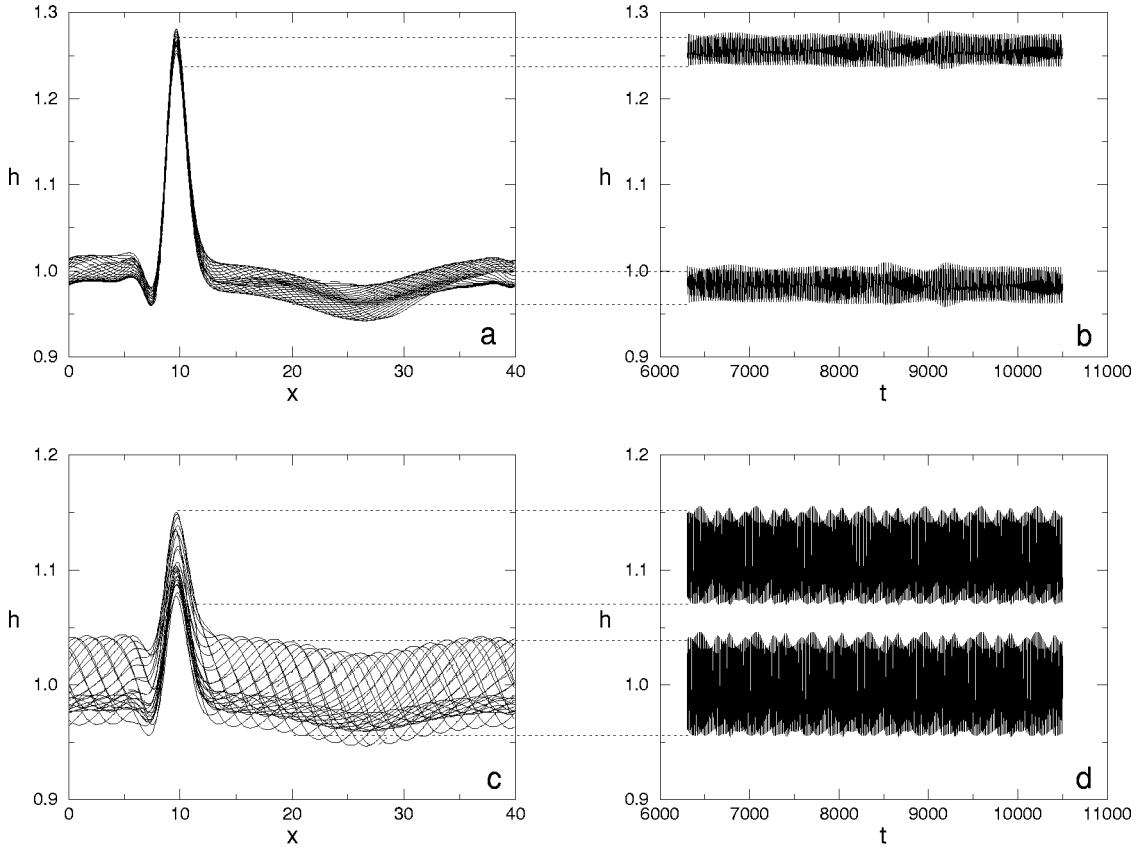


FIG. 18. The film dynamics as described by Eq. (8) with $S=5.69$, $B=0.1$, $M_w=15.4$, $\delta=0.5$, $L_w=5$, and $L_x=40$. For $R=1.5$ (a) the evolution of the liquid–gas interface from $t=10485$ (dashed curve) shown by increments of 0.5; (b) the time series of the film thickness at $x=10$ (the upper set) and $x=20$ (the lower set). For $R=3$ (c) same as (a); (d) same as (b). The dotted lines indicate the locations where the time series are recorded.

meinschaft under Grant No. TH781/1-1 and the Interuniversity Poles of Attraction Program IV-06, Belgium State, Federal Office for Scientific, Technical and Cultural Affairs. P.C. acknowledges financial support of the Fonds National de la Recherche Scientifique (Belgium). A.O. was partially supported by the Israel Science Foundation founded by the Israel Academy of Sciences and Humanities through Grant No. 369/99.

## APPENDIX: DERIVATION OF THE NONLINEAR EVOLUTION EQUATION

In this appendix a two-dimensional evolution equation describing the three-dimensional film dynamics will be derived. We start with the governing equations of the incompressible flow, which are, respectively, the Navier–Stokes, the energy balance and the continuity equations

$$\mathbf{v}_t+(\mathbf{v}\cdot\nabla)\mathbf{v}=-\frac{\nabla p}{\rho}+\nu\nabla^2\mathbf{v}+\mathbf{F}, \tag{A1}$$

$$T_t+\mathbf{v}\cdot\nabla T=\chi\nabla^2 T, \tag{A2}$$

$$\nabla\cdot\mathbf{v}=0, \tag{A3}$$

where $\mathbf{v}=\{u,v,w\}$, $T$ and $p$ are, respectively, the fields of velocity, temperature and pressure in the fluid, $\nabla=\{\partial_x,\partial_y,\partial_z\}$ is the gradient operator and $\mathbf{F}=\{g\sin\beta,0,-g\cos\beta\}$ is the body force. For the sake of simplicity the bars over the dimensional variables are here omitted.

At the free surface $z=h(x,y,t)$, the boundary conditions constitute the balance of the stresses, the Newton's cooling law and the kinematic condition,[2] respectively,

$$-(p-p_\infty)\mathbf{n}+2\mu\bar{\bar{P}}\cdot\mathbf{n}=2\sigma K\mathbf{n}+\nabla_s\sigma, \tag{A4}$$

$$-k\nabla T\cdot\mathbf{n}=\alpha_h(T-T_\infty), \tag{A5}$$

$$w=h_t+\mathbf{v}\cdot\nabla_s h, \tag{A6}$$

where $p_\infty$ and $T_\infty$ are the given pressure and temperature of the ambient air far from the liquid–gas interface, $\bar{\bar{P}}$ is the shear stress tensor in the liquid phase, $\mathbf{n}=\{-h_x,-h_y,1\}/\sqrt{1+h_x^2+h_y^2}$ is the unit normal vector, $\nabla_s$ is the surface gradient operator, and $K=-\frac{1}{2}\nabla\cdot\mathbf{n}$ is the mean interfacial curvature.

At the plate $z=0$ the boundary conditions are no-slip-no-penetration and a specified non-uniform temperature distribution, respectively,

$$\mathbf{v}=\mathbf{0}, \tag{A7}$$

$$T=T_a+T_w(x), \tag{A8}$$

where $T_a$ is the average temperature and $T_w(x)$ is a periodic temperature distribution in the flow direction with a zero average.

The dimensionless set of Eqs. (A1)–(A8) normalized using the scaling introduced in Sec. II with

$$y=\varepsilon\frac{\overline{y}}{h_N},\quad u=\frac{\nu\overline{u}}{h_N},\quad v=\frac{\nu\overline{v}}{h_N},\quad w=\varepsilon\frac{\nu\overline{w}}{h_N},\quad p=\frac{\rho\nu^2\overline{p}}{h_N^2},$$

reads

$$\begin{aligned}
&NSX\equiv\varepsilon u_t+\varepsilon uu_x+\varepsilon vu_y+\varepsilon wu_z+\varepsilon p_x\\
&\quad -R-\varepsilon^2u_{xx}-\varepsilon^2u_{yy}-u_{zz}=0,\\
&NSY\equiv\varepsilon v_t+\varepsilon uv_x+\varepsilon vv_y+\varepsilon wv_z+\varepsilon p_y\\
&\quad -\varepsilon^2v_{xx}-\varepsilon^2v_{yy}-v_{zz}=0,\\
&NSZ\equiv\varepsilon^2w_t+\varepsilon^2uw_x+\varepsilon^2vw_y+\varepsilon^2ww_z+p_z\\
&\quad +C-\varepsilon^3w_{xx}-\varepsilon^3w_{yy}-\varepsilon w_{zz}=0,\\
&EN\equiv\varepsilon T_t+\varepsilon uT_x+\varepsilon vT_y+\varepsilon wT_z\\
&\quad -\frac{1}{Pr}(\varepsilon^2T_{xx}+\varepsilon^2T_{yy}+T_{zz})=0,\\
&CO\equiv u_x+v_y+w_z=0,\\
&\underline{at\ \ z=h}\\
&HT\equiv\frac{1}{N}(\varepsilon^2h_xT_x+\varepsilon^2h_yT_y-T_z)-BT=0,\\
&CIN\equiv\varepsilon h_t+\varepsilon uh_x+\varepsilon vh_y-\varepsilon w=0,\\
&DYN\equiv p-\frac{2}{N}(\varepsilon^3h_x^2u_x+\varepsilon^3h_y^2v_y-\varepsilon u_x-\varepsilon v_y-\varepsilon h_xu_z\\
&\quad -\varepsilon^3h_xw_x-\varepsilon^3h_yw_y-\varepsilon h_yv_z+\varepsilon^3h_xh_yu_y\\
&\quad +\varepsilon^3h_xh_yv_x)+\frac{S}{\varepsilon^2}\frac{1}{N^3}(1-\varepsilon^2M_wCaT)(\varepsilon^2h_{xx}\\
&\quad +\varepsilon^4h_{xx}h_y^2+\varepsilon^2h_{yy}+\varepsilon^4h_{yy}h_x^2\\
&\quad -2\varepsilon^4h_{xy}h_xh_y)=0, \qquad \text{(A9)}\\
&DY1\equiv\frac{1}{N}(4\varepsilon^2h_xu_x+2\varepsilon^2h_xv_y-u_z-\varepsilon^2w_x+\varepsilon^2h_x^2u_z\\
&\quad +\varepsilon^4h_x^2w_x+\varepsilon^2h_yu_y+\varepsilon^2h_yv_x+\varepsilon^2h_xh_yv_z\\
&\quad +\varepsilon^4h_xh_yw_y)-\varepsilon M_w(T_x+h_xT_z)=0,\\
&DY2\equiv\frac{1}{N}(4\varepsilon^2h_yv_y+2\varepsilon^2h_yu_x)-\frac{\sqrt{1+\varepsilon^2h_y^2}}{\sqrt{1+\varepsilon^2h_x^2}}\\
&\quad \times(v_z+\varepsilon^2w_y-\varepsilon^2h_x^2v_z-\varepsilon^4h_x^2w_y-\varepsilon^2h_xu_y\\
&\quad -\varepsilon^2h_xv_x-\varepsilon^2h_xh_yu_z-\varepsilon^4h_xh_yw_x)\\
&\quad -\varepsilon M_w(T_y+h_yT_z)=0,\\
&\underline{at\ \ z=0}\\
&NS\equiv u=v=w=0,\\
&FT\equiv T-\delta-T_w(x)=0,
\end{aligned}$$

where $N=\sqrt{1+\varepsilon^2h_x^2+\varepsilon^2h_y^2}$ is the dimensionless metrics, $Ca=\rho\nu^2/\sigma_\infty h_N$ is the capillary number and $S=\varepsilon^2Ca^{-1}$.

By expanding the variables in power series of $\varepsilon$, with $\varepsilon\ll1$

$$\mathbf{r}\equiv\begin{pmatrix}u\\v\\w\\p\\T\end{pmatrix}=\mathbf{r_0}+\varepsilon\mathbf{r_1}+\varepsilon^2\mathbf{r_2}+\cdots, \qquad \text{(A10)}$$

and substituting them into Eqs. (A9), one obtains at each order a simplified set of equations. Further, the nonlinear system of Eqs. (A9) can be reduced to a single nonlinear evolution equation for the film thickness $h$. Here is the sequence of operations which leads to this evolution equation.

(i) We proceed with the asymptotic analysis by substituting Eqs. (A10) into the system of Eqs. (A9). Each of these equations is expanded in series with respect to $\varepsilon$. At leading order for $\varepsilon\to0$ a zeroth approximation of the governing system of equations is obtained as

$$\begin{aligned}
&NSX_0\equiv R+u_{0_{zz}}=0,\\
&NSY_0\equiv v_{0_{zz}}=0,\\
&NSZ_0\equiv C+p_{0_z}=0, \qquad \text{(A11)}\\
&EN_0\equiv T_{0_{zz}}=0,\\
&CO_0\equiv u_{0_x}+v_{0_y}+w_{0_z}=0,\\
&\underline{at\ \ z=h}\\
&HT_0\equiv T_{0_z}+BT_0=0,\\
&CIN_0\equiv h_t+u_0h_x+v_0h_y-w_0=0,\\
&DYN_0\equiv p_0+S(h_{xx}+h_{yy})=0,\\
&DY1_0\equiv u_{0_z}=0,\\
&DY2_0\equiv v_{0_z}=0,\\
&\underline{at\ \ z=0}\\
&NS_0\equiv u_0=v_0=w_0=0,\\
&FT_0\equiv T_0-\delta-T_w(x)=0.
\end{aligned}$$

(ii) Found by successive integrations the solution of Eqs. (A11) at leading order is

$$\begin{aligned}
&u_0=R\frac{z}{2}(2h-z),\\
&v_0=0,\\
&w_0=-R\frac{z^2}{2}h_x, \qquad \text{(A12)}\\
&p_0=C(h-z)-S(h_{xx}+h_{yy}),\\
&T_0=\delta+T_w(x)-BzT_i,
\end{aligned}$$

where

$$T_i=\frac{\delta+T_w(x)}{1+Bh},$$

is the interfacial temperature given by Eq. (5).

(iii) Substituting $u_0$ and $w_0$ into the kinematic boundary condition $CIN_0$ yields the leading order form of the evolution equation

$$h_t=-Rh^2h_x, \qquad \text{(A13)}$$

which describes the propagation of the liquid–gas interface down the plate. As follows from the linear

theory,[13] Eq. (15), $Rh^2$ is the phase speed of the interfacial wave which corresponds to twice the interface velocity of the film.

(iv) At first order of the asymptotic expansion in $\varepsilon$ we obtain

$$NSX_1 \equiv u_{0_t} + u_0 u_{0_x} + v_0 u_{0_y} + w_0 u_{0_z} + p_{0_x} - u_{1_{zz}} = 0,$$
$$NSY_1 \equiv v_{0_t} + u_0 v_{0_x} + v_0 v_{0_y} + w_0 v_{0_z} + p_{0_y} - v_{1_{zz}} = 0,$$
$$NSZ_1 \equiv p_{1_z} - w_{0_{zz}} = 0,$$
$$EN_1 \equiv T_{0_t} + u_0 T_{0_x} + v_0 T_{0_y} + w_0 T_{0_z} - \frac{1}{Pr} T_{1_{zz}} = 0,$$
$$CO_1 \equiv u_{1_x} + v_{1_y} + w_{1_z} = 0,$$
$$\underline{at \;\; z = h}$$
$$HT_1 \equiv T_{1_z} + BT_1 = 0,$$
$$CIN_1 \equiv u_1 h_x + v_1 h_y - w_1 = 0,$$
$$DYN_1 \equiv p_1 + 2(u_{0_x} + v_{0_y} + h_x u_{0_z} + h_y v_{0_z}) = 0, \quad \text{(A14)}$$
$$DY1_1 \equiv u_{1_z} + M_w (T_{0_x} + h_x T_{0_z}) = 0,$$
$$DY2_1 \equiv v_{1_z} + M_w (T_{0_y} + h_y T_{0_z}) = 0,$$
$$\underline{at \;\; z = 0}$$
$$NS_1 \equiv u_1 = v_1 = w_1 = 0,$$
$$FT_1 \equiv T_1 = 0.$$

(v) Found by successive integrations the solution of this system is

$$u_1 = \tfrac{1}{24} z[R^2 h_x h(z^3 - 4h^3) + 4R(z^2 - 3h^2) h_t - 24 M_w T_{i_x} + 12(z-2h)(Ch_x - S(h_{xxx} + h_{xyy}))],$$
$$v_1 = \tfrac{1}{2} z[-2M_w T_{i_y} + (z-2h)(Ch_y - S(h_{yyy} + h_{xxy}))],$$
$$w_1 = \tfrac{1}{120} z^2 [60C(h_x^2 + h_y^2) + 60M_w (T_{i_{xx}} + T_{i_{yy}}) + 20(z-3h)(S(h_{yyyy} + 2h_{xxyy}) - C(h_{xx} + h_{yy})) + 60Rhh_t h_x + R^2 h_x^2 (40h^3 - z^3) - 5Rh_{xt}(z^2 - 6h^2) - R^2 hh_{xx}(z^3 - 10h^3) - 60Sh_y(h_{yyy} + h_{xxy}) - 60Sh_x h_{xyy} - 60Sh_{xxx}(h + h_x) + 20Szh_{xxxx}], \quad \text{(A15)}$$
$$p_1 = -Rh_x(z+h),$$
$$T_1 = \tfrac{1}{120} Prz(20T_{i_t}(z(Bz-3) + (3Bz-6)h - 3Bh^2) + R(3Bz^4 - 5z^3 + 20h(z^2 - 2h^2) + 5Bhz^2(4h - 3z) - 15Bh^4 T_{i_x} + 20BT_i(h_t(3z - 6h) + Rhh_x(z^2 - 3h^2))).$$

(vi) In Eqs. (A15) the time-derivatives $h_t$, $h_{xt}$, and $T_{i_t}$ appear and are approximated at this order by using Eq. (A13).

(vii) We can now substitute $u_1$, $v_1$, and $w_1$ into the kinematic boundary condition $CIN_1$ to obtain the first-order in $\varepsilon$ correction for the evolution equation Eq. (A13).

Finally, the resulting evolution equation reads

$$h_t + Rh^2 h_x + \varepsilon \frac{2}{15} R^2 (h^6 h_x)_x + \varepsilon \nabla \cdot \left[ S \frac{h^3}{3} \nabla \nabla^2 h - C \frac{h^3}{3} \nabla h - M_w \frac{h^2}{2} \nabla T_i \right] + O(\varepsilon^2) = 0. \quad \text{(A16)}$$

We note that $T_1$ was not used to derive evolution equation Eq. (A16) up to $O(\varepsilon)$. This is different from the case studied by Miladinova *et al.*,[24,25] where $M_w = O(1/\varepsilon)$.


[1] L. E. Scriven and C. V. Sternling, "On cellular convection driven surface tension gradients effects of mean surface tension and surface viscosity," J. Fluid Mech. **19**, 321 (1964).
[2] P. Colinet, J. C. Legros, and M. G. Velarde, *Nonlinear Dynamics of Surface-Tension-Driven Instabilities* (Wiley, New York, 2000).
[3] C.-S. Yih, "Stability of liquid flow down an inclined plane," Phys. Fluids **6**, 321 (1963).
[4] T. B. Benjamin, "Wave formation in laminar flow down an inclined plane," J. Fluid Mech. **2**, 554 (1957).
[5] J. M. Floryan, S. H. Davis, and R. E. Kelly, "Instabilities of a liquid film flowing down a slightly inclined plane," Phys. Fluids **30**, 983 (1987).
[6] R. E. Kelly, D. A. Goussis, S. P. Lin, and F. K. Hsu, "The mechanism for surface wave instability in liquid film flow," Phys. Fluids A **1**, 819 (1989).
[7] M. K. Smith, "The mechanism for the long-wave instability in thin liquid films," J. Fluid Mech. **217**, 469 (1990).
[8] J. Liu, J. D. Paul, and J. P. Gollub, "Measurements of the primary instabilities of film flows," J. Fluid Mech. **250**, 69 (1993).
[9] J. Liu and J. P. Gollub, "Solitary wave dynamics of film flows," Phys. Fluids **6**, 1702 (1994).
[10] D. J. Benney, "Long waves on liquid films," J. Math. Phys. **45**, 150 (1966).
[11] A. Oron and O. Gottlieb, "Nonlinear dynamics of temporally excited falling liquid films," Phys. Fluids **14**, 2622 (2002).
[12] J. P. Burelbach, S. G. Bankoff, and S. H. Davis, "Nonlinear stability of evaporating/condensing liquid films," J. Fluid Mech. **195**, 463 (1988).
[13] S. W. Joo, S. H. Davis, and S. G. Bankoff, "Long-wave instabilities of heated falling films—two-dimensional theory of uniform layers," J. Fluid Mech. **230**, 117 (1991).
[14] A. Oron, S. H. Davis, and S. G. Bankoff, "Long-scale evolution of thin liquid films," Rev. Mod. Phys. **69**, 931 (1997).
[15] A. Pumir, P. Manneville, and Y. Pomeau, "On solitary waves running down an inclined plane," J. Fluid Mech. **135**, 27 (1983).
[16] P. Rosenau, A. Oron, and J. M. Hyman, "Bounded and unbounded patterns of the Benney equation," Phys. Fluids A **4**, 1102 (1992).
[17] V. Ya. Shkadov, "Wave flow regimes of a thin layer of viscous fluid subject to gravity," Akad. Nauk SSSR, Mekh. Zhidk. Gaza **2**, 43 (1967).
[18] C. Ruyer-Quil and P. Manneville, "Improved modeling of flows down inclined planes," Eur. Phys. J. B **15**, 357 (2000).
[19] C. Ruyer-Quil and P. Manneville, "Further accuracy and convergence results on the modeling of flows down inclined planes by weighted-residual approximations," Phys. Fluids **14**, 170 (2002).
[20] M. J. Tan, S. G. Bankoff, and S. H. Davis, "Steady thermocapillary flows of thin liquid layers," Phys. Fluids A **2**, 313 (1990).
[21] S. J. VanHook, M. F. Schatz, J. B. Swift, W. D. McCormick, and H. L. Swinney, "Long-wavelength surface-tension-driven Bénard convection experiment and theory," J. Fluid Mech. **345**, 45 (1997).
[22] A. C. Or, R. E. Kelly, L. Cortelezzi, and J. L. Speyer, "Control of long-wavelength Marangoni–Bénard convection," J. Fluid Mech. **387**, 321 (1999).
[23] O. A. Kabov, "Heat transfer from a heater with small linear dimension to free falling liquid film," Proceedings of the First Russian National Conference on Heat Transfer **6**, 90 (1994).
[24] S. Miladinova, S. Slavtchev, G. Lebon, and J. C. Legros, "Long-wave instabilities of nonuniformly heated falling films," J. Fluid Mech. **453**, 153 (2002).
[25] S. Miladinova, D. Staykova, G. Lebon, and B. Scheid, "Effect of nonuniform wall heating on the three-dimensional secondary instability of falling films," Acta Mech. **156**, 79 (2002).

[26]B. Scheid, O. A. Kabov, C. Minetti, P. Colinet, and J. C. Legros, ''Measurement of free surface deformation by reflectance-Schlieren method,'' Proc. 3rd Eur. Thermal-Sci. Conf., Heidelberg **2**, 651 (2000).
[27]O. A. Kabov, B. Scheid, I. A. Sharina, and J. C. Legros, ''Thermocapillary convection in a falling thin liquid film locally heated,'' Proc. 5th World Conf. Exp. Heat Transfer, Fluid Mech. and Thermodynamics, Thessaloniki, **3**, 2007 (2001).
[28]I. V. Marchuk and O. A. Kabov, ''Numerical modeling of thermocapillary reverse flow in thin liquid films under local heating,'' Russ. J. Eng. Thermophys. **8**(1–4), 17 (1998).
[29]O. A. Kabov, B. Scheid, I. V. Marchuk, and J. C. Legros, ''Free surface deformation by thermocapillary convection in a flowing locally heated thin liquid layer,'' Mechanica Zhidkosti i Gaza **3**, 200 (2001).
[30]J. M. Skotheim, U. Thiele, and B. Scheid, ''On the instability of a falling film due to localized heating,'' J. Fluid Mech. (to be published).
[31]O. A. Kabov, I. V. Marchuk, and V. M. Chupin, ''Thermal imaging study of the liquid film flowing on vertical surface with local heat source,'' Russ. J. Eng. Thermophys. **6**(2), 104 (1996).
[32]I. V. Marchuk and O. A. Kabov, ''Numerical simulation of heat transfer in a falling liquid film with allowance for heat conduction in heaters,'' Russ. J. Eng. Thermophys. **10**(2), 147 (2000).
[33]S. W. Joo, S. H. Davis, and S. G. Bankoff, ''A mechanism for rivulet formation in heated falling films,'' J. Fluid Mech. **321**, 279 (1996).
[34]B. Ramaswamy, S. Krishnamoorthy, and S. W. Joo, ''Three-dimensional simulation of instabilities and rivulet formation in heated falling films,'' J. Comput. Phys. **131**, 70 (1997).
[35]E. Doedel, A. Champneys, T. Fairfrieve, Y. Kuznetsov, B. Sandstede and X. Wang, ''AUTO 97 Continuation and bifurcation software for ordinary differential equations,'' Montreal Concordia University (1997).
[36]A. Oron and S. G. Bankoff, ''Dynamics of a condensing liquid film under disjoining–conjoining pressures,'' Phys. Fluids **13**, 1107 (2001).
[37]T. R. Salamon, R. C. Armstrong, and R. A. Brown, ''Traveling waves on vertical films: Numerical analysis using the finite element method,'' Phys. Fluids **6**, 2202 (1994).
[38]L. T. Nguyen and V. Balakotaiah, ''Modeling and experimental studies of wave evolution on free falling viscous films,'' Phys. Fluids **12**, 2236 (2000).